

χ -Systems for Correlation Functions

J. Caetano^{a,b,c}, J. Toledo^{a,b}

^a*Perimeter Institute for Theoretical Physics
Waterloo, Ontario N2L 2Y5, Canada*

^b*Department of Physics and Astronomy & Guelph-Waterloo Physics Institute,
University of Waterloo, Waterloo, Ontario N2L 3G1, Canada*

^c*Centro de Física do Porto e Departamento de Física e Astronomia,
Faculdade de Ciências da Universidade do Porto,
Rua do Campo Alegre, 687, 4169-007 Porto, Portugal*

jd.caetano.s, jonathan.campbell.toledo@gmail.com

Abstract

We consider the strong coupling limit of 4-point functions of heavy operators in $\mathcal{N} = 4$ SYM dual to strings with no spin in AdS. We restrict our discussion for operators inserted on a line. The string computation factorizes into a state-dependent sphere part and a universal AdS contribution which depends only on the dimensions of the operators and the cross ratios. We use the integrability of the AdS string equations to compute the AdS part for operators of arbitrary conformal dimensions. The solution takes the form of TBA-like integral equations with the minimal *AdS* string-action computed by a corresponding free-energy-like functional. These TBA-like equations stem from a peculiar system of functional equations which we call a χ -system. In principle one could use the same method to solve for the *AdS* contribution in the N -point function. An interesting feature of the solution is that it encodes multiple string configurations corresponding to different classical saddle-points. The discrete data that parameterizes these solutions enters through the analog of the chemical-potentials in the TBA-like equations. Finally, for operators dual to strings spinning in the same equator in S^5 (i.e. BPS operators of the same type) the sphere part is simple to compute. In this case (which is generically neither extremal nor protected) we can construct the complete, strong-coupling 4-point function.

Contents

1	Introduction	3
2	Four point function generalities	6
3	AdS_2 Pohlmeyer reduction	8
3.1	Equations of motion and stress-energy tensor	8
3.2	The function γ	10
3.3	Spikes, fold-lines and string embeddings	11
3.4	The action as a wedge product	12
4	The linear problem	14
4.1	Basic properties	14
4.2	Defining solutions globally	16
4.3	WKB approximation and WKB Curves	17
4.4	WKB triangulation	19
4.5	Coordinates	21
4.6	WKB asymptotics of the coordinates	25
4.7	Shift relation.	26
4.8	χ -system.	27
4.9	Inverting χ -systems	29
4.10	Extracting η -cycles	30
5	The AdS action	31
5.1	Regularized AdS action	31
5.1.1	Stress-energy tensor and WKB triangulation	32
5.1.2	χ -system for the 4-point function	32
5.1.3	Finite part of AdS action	34
5.1.4	Numerical tests	35
5.2	Divergent part	37
5.2.1	Reconstruction formulas	37
5.2.2	Physical regulator and spacetime dependence	38
5.3	Summary of the AdS and divergent contributions	39

6	Full correlation function for BMN operators	40
6.1	Sphere part	40
6.2	Saddle point determination	41
6.3	Saddle points and multiple string configurations	43
6.4	Extremal Limit	44
7	Discussion and future directions	46
A	The linear problem	48
A.1	Summary of the linear problem	48
A.2	Solutions near w_a	49
A.3	Solutions near z_a	50
B	WKB analysis	50
B.1	Statement of the WKB approximation	50
B.2	Subleading WKB	51
B.3	WKB expansion of the coordinates	53
C	Fold lines and Properties of γ	54
C.1	Fold lines	54
C.2	Structure of γ near w_a	55
C.3	Structure of contours where $\gamma = 0$	56
D	Details of the 4-point function computation	58
D.1	Explicit expression for stress-energy tensor coefficients	58
D.2	Explicit expressions for χ -functions and A_{PQ}	58
D.3	Finite part of AdS	59
E	Three-point function in GMN language	61

1 Introduction

One of the most interesting objects to study in an interacting quantum field theory is the four-point function. In conformal field theories these are the first N -point functions whose spacetime dependence is not explicitly fixed by conformal symmetry. The computation of this correlator is generally highly nontrivial and obtaining explicit expressions outside the

perturbative regime is typically impossible. However, the advent of the AdS/CFT correspondence has made it possible to access the strong coupling limits of special QFT's. In particular the correspondence [1] maps the strong coupling limit of $\mathcal{N} = 4$ SYM to a theory of classical strings moving in an $AdS_5 \times S^5$ background. This allows the computation of leading strong coupling behavior of certain 4-point functions in $\mathcal{N} = 4$ SYM, which is the main purpose of this paper. While we have mostly focused on the 4-point computation, we note that the method used below could in principle be applied for the corresponding N -point computation.

There are also interesting indirect applications. One of our main motivations for this work is the possibility of exploring the spectrum and the structure constants of $\mathcal{N} = 4$ SYM through the operator product expansion (OPE) of the four point function. Another potentially interesting application of this calculation is in the weak-strong coupling connections reported in [2, 3, 4, 5, 6] that suggests the existence of an underlying common structure in both regimes.

At strong coupling, the problem of computing the correlation function is that of finding the area of the minimal surface in $AdS_5 \times S^5$ that goes to the AdS boundary at the operator insertion points x_a . In this paper, we compute the AdS part of the correlation function for arbitrary heavy scalar operators inserted along a line. The method used here is inspired by the integrability techniques originally developed for the Null Polygonal Wilson loop problem [10] and later applied to the computation of three-point functions [8, 9, 11]. As in these previous applications, integrability allows one to compute the minimal AdS action without knowing the explicit classical solution. For the four point correlation function the connection with Hitchin systems and the formalism developed in [12] is used intensely. As in [10, 8, 9] the starting point of the method is the map of the string equations of motion in AdS to a certain the auxilliary linear problem by Pohlmeyer reduction. Ultimately the solution takes the form of a set of functional equations that we call a χ -system. These functional equations are similar in spirit to the Y -system appearing in [10] and which naturally arise in the solutions of integrable QFT's.

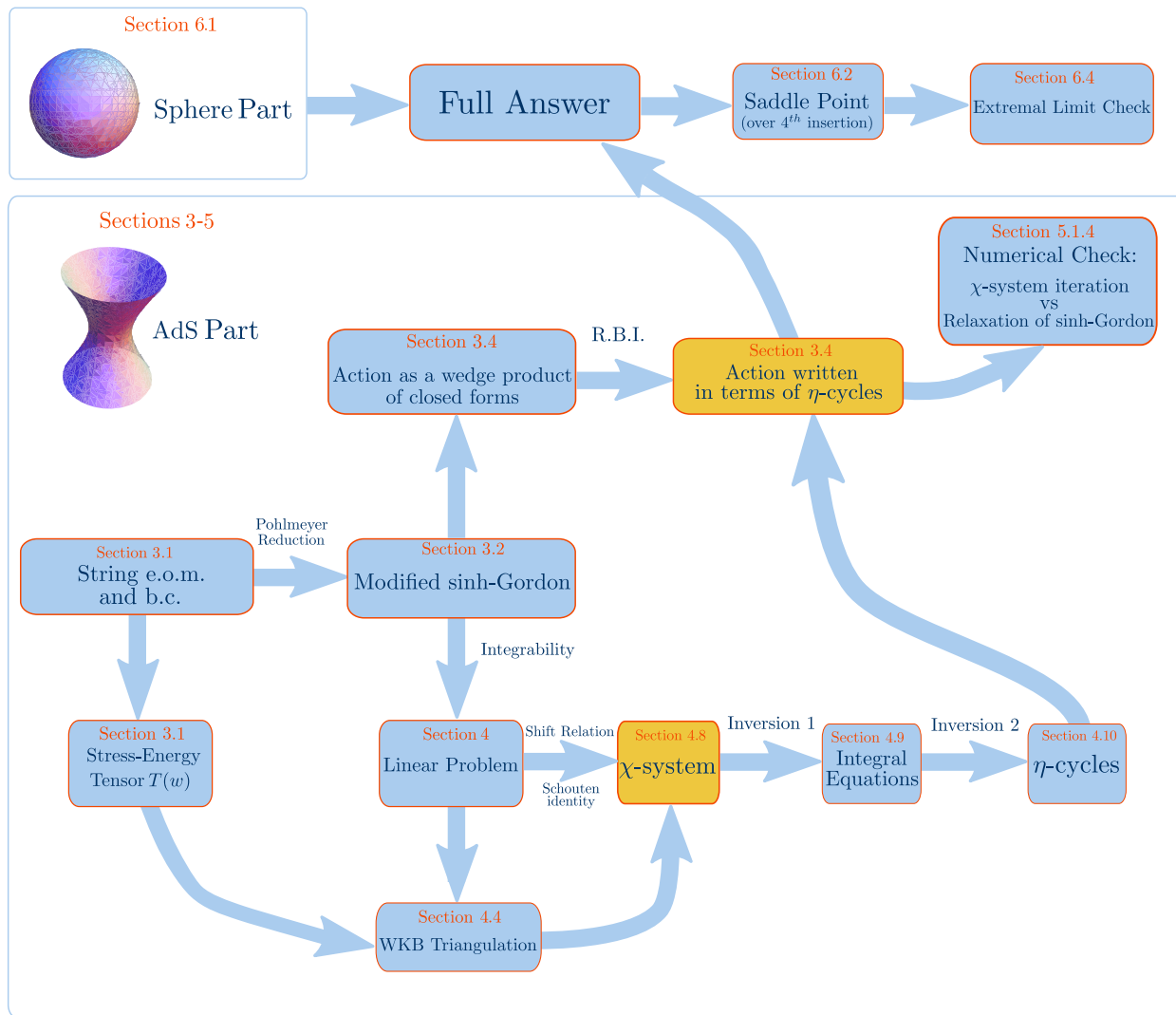
For some specific BPS operators dual to strings spinning on the same great circle of S^5 the sphere contribution is well know. In this case we can construct the full strong-coupling correlation function. We emphasize that these 4-point functions are generically neither extremal nor protected. Complete, non-protected results for correlation functions of heavy operators at strong coupling are quite rare. For example, in [8], the AdS part of the three-point function is computed, but the only case for which the sphere is known (BPS operators) is protected. The only complete, non-protected result that we know of is [11] where the strong-coupling three-point functions of GKP strings is computed.¹

The layout of the paper is as follows. In the section 2 we start by giving the general strategy of this work and discuss some physically relevant aspects of the problem. Then, in section 3 we write the AdS part of the correlation function in terms of objects which are naturally computed using the integrability of the string equations of motion. In section 4 we introduce a formalism that will lead to the χ -system which is the set of functional equations

¹Using the results of this paper it may be possible to extend the results of [11] to the complete N -point functions of GKP strings at strong coupling since the mathematical problem is similar to the one treated here.

that allows one to compute the minimal AdS action. In section 5 we compute explicitly the AdS part of the correlation function using the χ -system and explain the mechanism by which the dependence on the spacetime points emerges. We also present some numerical tests of the results. In section 6.1, we compute the sphere part for the specific case of BPS operators with large charges. In section 6.2, we discuss the saddle points of the fourth insertion point of the correlation function and perform some numerical studies on this issue. In the same section, we study the extremal limit of the correlation function which is an analytical test of the result. In section 7 we conclude and discuss some open problems.

Finally, because the computation involves many intermediate steps in the flow-chart below we summarize for the reader the basic components of the method. The flow-chart provides a map of the paper and summarizes the main steps of the computation which are shown in the individual boxes. Each box contains a reference to the relevant section where that part of the computation is discussed.



2 Four point function generalities

For large 't Hooft coupling λ , the semi-classical computation of correlation functions corresponds to the evaluation of the AdS_5 and S^5 actions for classical solutions with the topology of a four punctured sphere. The boundary conditions are that the solution close to each puncture P_a , which is associated with the gauge theory operator $\mathcal{O}_a(x_a)$, approaches the AdS boundary at the point x_a in the same way as a 2-point function involving $\mathcal{O}_a(x_a)$ and some other heavy, scalar operator. In this paper, we study the simplest case where the operators are inserted on a line in \mathbb{R}^4 . This implies that the string solution is contained in a Euclidean AdS_2 subspace of AdS_5 . Moreover, there is only one independent cross-ratio. The conformal symmetry of $\mathcal{N} = 4$ constrains the four-point correlation function to take the form

$$\langle \mathcal{O}_1(x_1)\mathcal{O}_2(x_2)\mathcal{O}_3(x_3)\mathcal{O}_4(x_4) \rangle = f(u) \prod_{a>b}^4 (x_{ab})^{\Delta_{ab}}, \quad (1)$$

where $x_{ab} = x_a - x_b$, Δ_a is the dimension of operator \mathcal{O}_a , $\Delta_{ab} = (\sum_c \Delta_c) / 3 - \Delta_a - \Delta_b$ and u is the conformal cross-ratio

$$u = \frac{x_{14}x_{23}}{x_{12}x_{34}} \quad (2)$$

Both the AdS and sphere contributions contain divergences as the string approaches the position of the operators at the boundary of AdS , which requires a cut-off $z = \mathcal{E}$. To describe the world-sheet we use complex variables w, \bar{w} . On the 4-punctured sphere, the physical cut-off \mathcal{E} corresponds to cutting out small disks of radius ϵ_a around each puncture P_a at w_a . Ultimately, we will need to establish a precise relation between the cut-off's ϵ_a and \mathcal{E} . As we will review later, this is possible given the data accessible from integrability [8].

In this paper, we will consider operators with charges scaling as $\sqrt{\lambda}$, and without spin in AdS . Following the prescription developed in [7, 8], we account for the states in the sphere by introducing an extra contribution of wave-functions. Therefore, the semi-classical four-point function is given schematically by

$$\int dw_4 e^{-\frac{\sqrt{\lambda}}{\pi} \int_{\Sigma \setminus \{\epsilon_a\}} \mathcal{L}_{AdS_2}} e^{-\frac{\sqrt{\lambda}}{\pi} \int_{\Sigma \setminus \{\epsilon_a\}} \mathcal{L}_{S^5}} \Psi_1 \Psi_2 \Psi_3 \Psi_4 \quad (3)$$

where the actions are evaluated on a classical (Euclidean) string solution approaching the boundary of AdS at the positions of the insertion points x_a .

In principle, there is an integral over all four insertion-points on the worldsheet. In (3) we only integrate over the insertion w_4 since the position of the other punctures can be fixed by conformal transformations. Since we are considering the $\lambda \rightarrow \infty$ limit, one can evaluate the integral over w_4 by saddle point and the end result is the integrand of (3) evaluated at the dominant saddle point.

Let us consider the issue of the saddle point in some detail since it will be an interesting aspect of our computation. There are two issues here: the positions of the operators on the boundary and the positions of the insertion points on the sphere. We can use the target-space conformal symmetry to place three of the operators at $x_1 = 1$, $x_2 = \infty$, $x_3 = -1$ and the world-sheet conformal symmetry to fix $w_1 = 1$, $w_2 = \infty$, $w_3 = -1$. The position x_4 is an

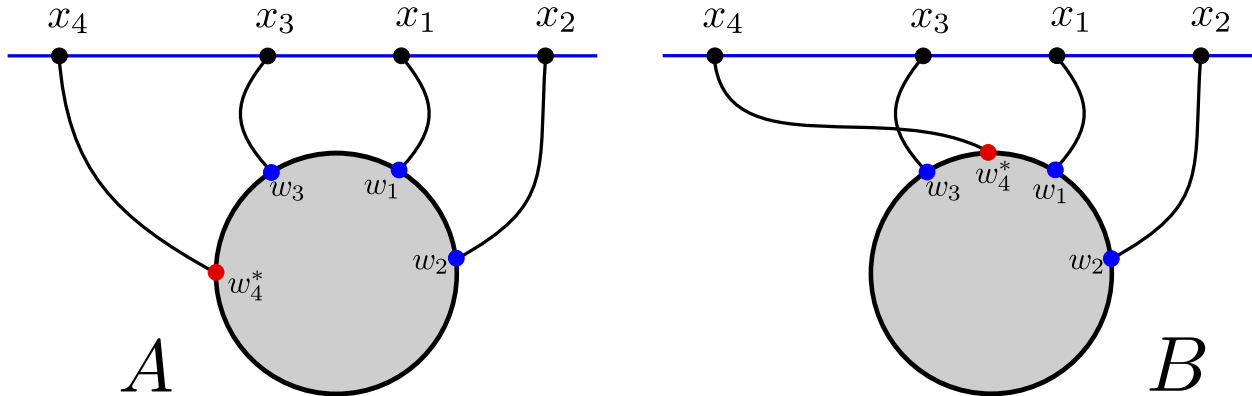


Figure 1: Insertions on the 4-punctured sphere. The gray ball represents the world-sheet (the complex plane plus the point at infinity, or simply ‘the sphere’) and the black boundary of the ball represents the equator of the sphere. The points w_a are the punctures on the sphere corresponding to the operators inserted at the positions x_a at the boundary of AdS_2 , which is represented by the straight line. We fix the points w_1, w_2, w_3 and x_1, x_2, x_3 using the world-sheet and target-space conformal symmetry respectively. The position of the fourth insertion w_4 should be fixed at the dominant saddle point w_4^* of the integrand of (3). By symmetry we expect this saddle point to also be along the real axis, and thus we have a notion of an ordering of the 4 punctures (but see footnote 2). In particular, there is three distinct ranges for the location of w_4^* . Consider the ordering of the x_a shown in this figure. If the dominant saddle point is located between w_2 and w_3 (as in panel A) then the insertions will not cross and the string embedding will look schematically like the one shown in figure 2A. If the dominant saddle-point is located between w_3 and w_1 (as in panel B) or between w_1 and w_2 then the insertions cross each-other and we expect the string embedding to look like the one shown in figure 2B.

input since we can put \mathcal{O}_4 anywhere along the line that contains $\mathcal{O}_{1,2,3}$. On the other hand, once we choose x_4 the position of the fourth puncture is fixed at $w_4 = w_4^*$ by the saddle-point condition. By symmetry we expect the dominant saddle-point to be located on the real axis and in this case we have a notion of an ordering of the punctures.² In particular, there are three possible in-equivalent orderings depending on the position of w_4 . Figure 1 shows two of these possibilities. If the ordering of the x_a is the same as the w_a then the insertions do not cross each other, as in figure 1A. If the ordering of the x_a is different from that of the w_a , then the insertions will cross as in figure 1B. These two possibilities lead to two types of string embeddings with distinctly different properties as is shown in figure 2. We will see that two types of solutions arise naturally in our construction. We are able to characterize the qualitative features of the spacetime embeddings and compute the minimal AdS action of both types of solutions. We will return to this topic below.

²We have confirmed numerically that there are saddle points along the real axis. There may also be the possibility saddle points off of the real axis and occurring in complex-conjugate pairs, but we have not investigated this possibility. This issue certainly requires further investigation.

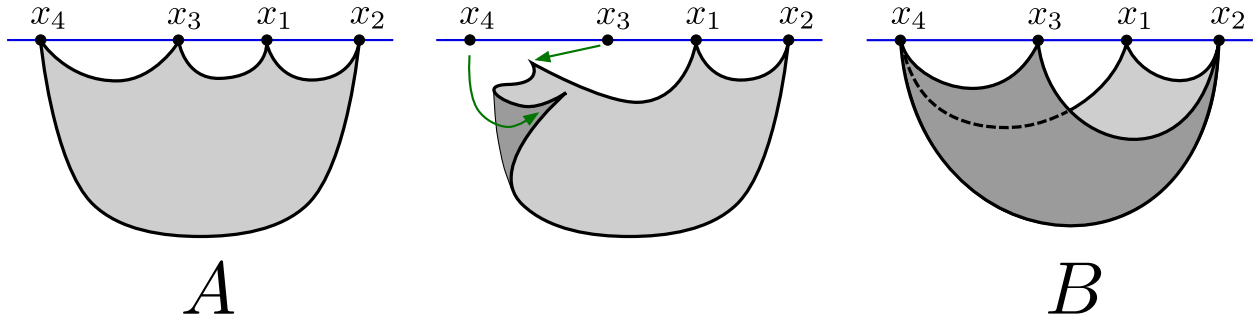


Figure 2: Two different possible string embeddings in AdS_2 which obey the required boundary conditions. These two solutions are shown in panels A and B. The center panel shows how to generate the configuration of panel B from that of panel A by interchanging the order in which the insertions on the sphere attach to the boundary; this interchange results in the characteristic folding shown in the embedding of panel B. These two types of solutions arise from the possibility that for a given choice of operator insertion points x_a the insertion point w_4^* (see figure 1) can be located in any of the three possible intervals (w_2, w_3) , (w_3, w_1) , (w_1, w_2) .

3 AdS_2 Pohlmeyer reduction

In this section we briefly review the Pohlmeyer-reduction process. We begin with a discussion of the string equations of motion and the stress-energy tensor, which is the starting point of the reduction. We then introduce the function γ in terms of which the AdS Lagrangian can be written. It turns out that γ satisfies a non-linear but *scalar* equation of motion that is a modified version of the well-know sinh-Gordon equation. Next we show how the different types of string embeddings discussed in section 2 are encoded though the boundary conditions imposed on γ . Finally we use the function γ to write the AdS action in a form where integrability is more readily applied.

3.1 Equations of motion and stress-energy tensor

Recall that we can consider (euclidean) AdS_2 as a surface in $R^{1,2}$ obeying the constraint

$$Y \cdot Y = (Y_1)^2 - (Y_2)^2 + (Y_3)^2 = -1. \quad (4)$$

We write the action for a string in AdS_2 as

$$S = \frac{1}{2} \int d^2\sigma [\partial_\alpha Y \cdot \partial^\alpha Y + \lambda(Y \cdot Y + 1)] \quad (5)$$

and the resulting equations of motion as

$$\square Y = (\partial Y \cdot \bar{\partial} Y) Y \quad (6)$$

The first term in the action is just the free string action in $R^{1,2}$; the second term is a Lagrange multiplier term that imposes (4).

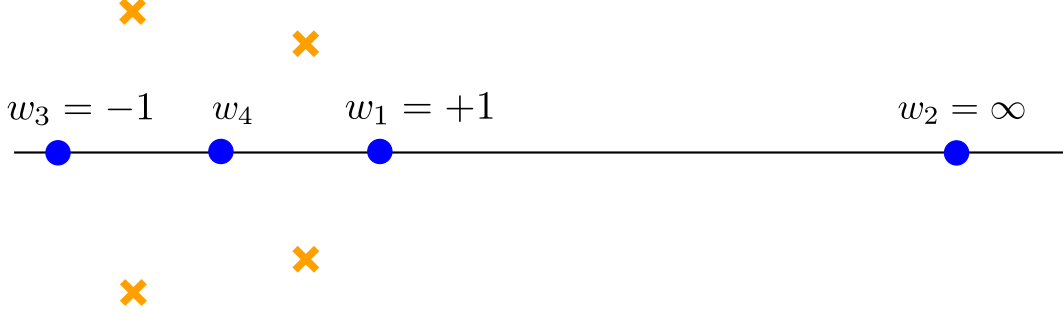


Figure 3: Schematic analytic structure of T . The blue dots represent the (double) poles of T at locations w_a and corresponding to the operator insertions $\mathcal{O}_a(x_a)$. The yellow crosses indicated zeros of T . We have fixed the positions of w_1 , w_2 and w_3 using the world-sheet conformal symmetry. We have arbitrarily placed w_4 in the interval (w_3, w_1) although generically the saddle-point w_4^* can be located in any of the three intervals along the real axis.

The equations of motion (6) must be supplemented by the Virasoro constraints and boundary conditions. The Virasoro constraint requires $T_{AdS} + T_S = 0$. In particular, the AdS contribution to the stress-energy tensor does not vanish. Fortunately the boundary conditions allow us to completely fix the form of $T_{AdS} = -T_S$. Here we are interested in solutions with the topology of a four-punctured sphere where the punctures are at the position of the operator insertions and thus the boundary conditions give the behavior of the string solutions near the insertion points. The correct prescription is to demand that the string goes to the boundary at the insertion points. Furthermore, it should approach the boundary in a specific way as dictated by the vertex operators. The behavior of the solution near the boundary will be dominated by the operator inserted there, independent of the properties or number of other operators inserted at different points. This means that the behavior near the insertion points can be determined from the 2-point function, where the string solution is known explicitly. From the explicit solution for the 2-point function one finds that the desired property of the solution near insertion point w_a is [8]

$$(\partial Y)^2 \equiv T(w) \sim \frac{\Delta_a^2}{4(w - w_a)^2} \quad (w \rightarrow w_a) \quad (7)$$

where $T(w)$ is the holomorphic component of T_{AdS} . The corresponding property also is required for the anti-holomorphic component $\bar{T}(\bar{w})$. Thus we know that T should be an analytic function on the (4-punctured) Riemann sphere with double-pole singularities at the punctures. This fixes T to be a specific rational function.

First consider the denominator of the rational function T . The polynomial in the denominator is determined by the positions of the insertions. Three of the insertions can be fixed by conformal symmetry, leaving one final insertion. The integrand of (3) will be a function of this final insertion point. In the limit $\sqrt{\lambda} \rightarrow \infty$ the integral localizes at the saddle point $w_4 = w_4^*$, thus fixing completely the denominator of T .

Now consider the numerator of T . Without loss of generality we can consider the case where there is no insertion at infinity since we can perform a transformation that maps any arbitrary point to infinity. Then the polynomial in the numerator can be at most of degree 4

(otherwise T would not be regular at infinity) and therefore it is characterized by 5 parameters. Four of these parameters are fixed by the condition (7). The final unfixed parameter, which we will call U , parameterizes the single cross-ratio of the four operators (recall that four points in a line have only one independent cross-ratio). The precise map between the parameter U and the cross-ratio u is quite involved but fortunately we will not need it since the cross-ratio will be encoded in the χ -system in a simple way. The analytic structure of T is shown schematically in figure 3. We will use this sort of figure to represent T throughout this paper.

3.2 The function γ

Our objective is to evaluate the AdS part of the string action. In Poincaré coordinates the on-shell action becomes³

$$\partial Y \cdot \bar{\partial} Y = \frac{\partial x \bar{\partial} x + \partial z \bar{\partial} z}{z^2} = \sqrt{T\bar{T}} \cosh \gamma \quad (9)$$

where the above formula defines the function $\gamma(w, \bar{w})$. It follows from the equations of motion that γ satisfies the modified sinh-Gordon equation

$$\partial \bar{\partial} \gamma = \sqrt{T\bar{T}} \sinh \gamma. \quad (10)$$

It is well known that this equation is classically integrable, and in what follows we exploit this integrability to compute the AdS action.

Now let us determine what boundary conditions should be imposed on γ . For the 2-point function $\gamma = 0$. Recall that the string solution should approach that of the 2-point function as the string approaches the boundary at the operator insertion points x_a . Therefore we should require that $\gamma \rightarrow 0$ as $w \rightarrow w_a$ [8]. Furthermore, in order to have a non-singular world-sheet metric the right-hand side of (9) should never vanish. Thus when T has a zero γ must have a logarithmic singularity to cancel it. In summary, the boundary conditions on γ are

$$\gamma \rightarrow \pm \frac{1}{2} \log T\bar{T} \quad (w \rightarrow z_a) \quad (11)$$

$$\gamma \rightarrow 0 \quad (w \rightarrow w_a) \quad (12)$$

where z_a denotes a zero of T and w_a a pole of T . Notice that the regularity of the world-sheet metric does not fix the sign of the logarithmic ‘spike’ in (11) and, in principle, different choices are possible at each zero (recall that generically T will have 4 zeros for the 4-point function, as follows from the discussion of the previous section). These different choices correspond to different string solutions having differing properties, and generically different

³The AdS_2 Poincaré coordinates are given by

$$Y^1 = -\frac{1}{2z} (1 - x^2 - z^2), \quad Y^2 = \frac{1}{2z} (1 + x^2 + z^2), \quad Y^3 = \frac{x}{z}. \quad (8)$$

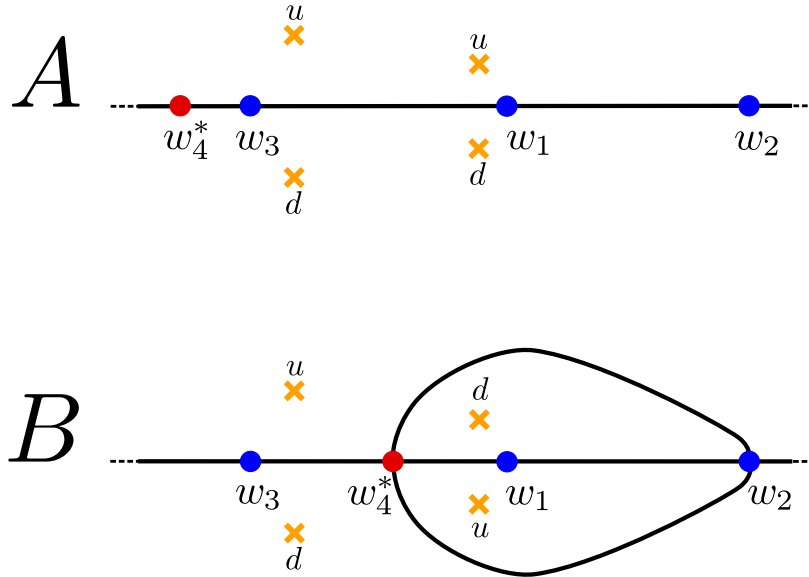


Figure 4: Contours where $\gamma = 0$ based on the choice of signs in equation (11). These contours are shown schematically by the black curves. The label u (d) at a zero indicates the choice of sign $+$ ($-$) in equation (11). We give a detailed discussion of why these are the only possible structures for these contours in appendix C. The key in relating these figures to the embeddings in figure 2 is that contours on the world-sheet where $\gamma = 0$ map onto folds of the embedding.

total action. We will refer to the spikes with the $+$ ($-$) sign as u -spikes (d -spikes). We will now describe how the choice of these signs is related to the string embeddings shown in figure 2.

3.3 Spikes, fold-lines and string embeddings

As mentioned in the previous section there are 4 zeros of T and at each zero we have a \mathbb{Z}_2 ambiguity (see equation (11)) in the choice of spikes of γ . A priori there are 2^4 different choices for the spikes. However, it turns out that there are only 2 distinct choices that correspond to target-space solutions with the desired properties. These two possibilities are shown in figure 4. A discussion of why these are the only two possible choices is given in appendix C.⁴ These two different possibilities correspond precisely to the two different possible string solutions shown in figure 2. The key ingredient in making this correspondence is the observation that contours on the world-sheet where $\gamma = 0$ correspond to fold-lines in the string embedding (see appendix C). The location of these contours is directly connected with the choice of spikes. For example, between a u -spike and a d -spike we know that there must be at least one such contour. In figure 4 the $\gamma = 0$ contours are indicated by the black curves. In appendix C we discuss in detail how the structure of these contours is inferred

⁴The main ideas are: first, configurations related by $\gamma \rightarrow -\gamma$ are not distinct since this is a symmetry of (10), and second, one should choose the spikes such that $\gamma \rightarrow -\gamma$ under reflection about the real axis. See appendix C.

from the choice of spikes.

Let us describe in more detail how we relate the two spike configurations in figure 4 to the two string embeddings in figure 2. As mentioned above, the key ingredient is to study the fold lines in the two figures. First consider the target-space solution. In figure 2A it is clear that there is a single fold-line that runs through each of the punctures in sequence. That is, there is a fold-line directly connecting x_4 with x_3 then x_3 with x_1 , etc. This is in agreement with the fold-structure implied by figure 4A since for this choice of spikes we can deduce that there is a single contour where $\gamma = 0$ running along the real axis connecting w_4 to w_3 then w_3 to w_1 , etc. Thus the spike configuration of figure 4 describes a string embedding of the type shown in figure 2A.

Now consider the folds of the embedding shown in figure 2B. Insertions x_1 and x_3 are both connected by fold lines directly to the insertions x_2 and x_4 . Furthermore, x_2 and x_4 are connected to each other by *two* fold-lines. This is because this configuration is double-folded along that line, as one can see from the construction shown in the center panel of figure 2. All of this is in perfect agreement with the fold-structure implied by figure 4B. In particular, for this choice of spikes both w_1 and w_3 are directly connected to w_2 and w_4^* by contours where $\gamma = 0$. Moreover, w_2 and w_4^* are connected by *two* contours where $\gamma = 0$, precisely corresponding to the double-fold line connecting x_2 and x_4 in figure 2B.

Let us comment on a subtle point regarding figure 4. Note that we have placed the saddle point w_4^* in different intervals in the two figures. On one hand, we should do this in order to be in agreement with figures 1 and 2. However, as we will see, given a cross-ratio u and the saddle point w_4^* , the fold structure is fixed. So, to compare two different fold structures for a given cross ratio we are forced to place the saddle point w_4^* in different intervals. This is in perfect agreement with the intuitive perspective of figures 1 and 2. We will return to this point in section 6.3.

3.4 The action as a wedge product

We will now return to the computation of the minimal AdS action (see equation (3)). Explicitly, the quantity we want to evaluate is

$$-\frac{\sqrt{\lambda}}{\pi} \int_{\Sigma \setminus \{\epsilon_a\}} \frac{\partial x \bar{\partial} x + \partial z \bar{\partial} z}{z^2} \quad (13)$$

where $\Sigma \setminus \{\epsilon_a\}$ denotes the sphere with small disks of radius ϵ_a cut out at each puncture. These cut-offs are not independent and are all fixed in terms of the single target-space cut-off $z = \mathcal{E}$; this is important in recovering the spacetime dependence of the correlation function and we will return to this point below [8]. It is convenient to separate the action into a piece that is independent of the cut-offs, and a piece where the dependence can be explicitly evaluated. This can be done because the solution near the punctures is known. In particular, we may write [10, 8]

$$\mathcal{A} = -\frac{\sqrt{\lambda}}{\pi} \int_{\Sigma} \sqrt{TT} (\cosh \gamma - 1) - \frac{\sqrt{\lambda}}{\pi} \int_{\Sigma \setminus \{\epsilon_a\}} \sqrt{TT} \quad (14)$$

To extend the integration to the full sphere in the first term we have used the fact that the action (9) goes like \sqrt{TT} near the punctures as follows from (12). We will refer to the

first and second term in (14) as A_{fin} and A_{div} respectively. Since T is known A_{div} can be evaluated explicitly in terms of the ϵ_a , but to eliminate the ϵ_a in terms of \mathcal{E} requires detailed information about the string solution itself. Fortunately, the tools necessary for computing A_{fin} will also provide the necessary information to complete the calculation of A_{div} . Thus, let us focus for the time being on the computation of A_{fin} and return to A_{div} afterwards.

We would like to write A_{fin} in a form where the integrability of (10) is more readily usable. Following [10, 8] we introduce the forms

$$\omega = \sqrt{T} dw \tag{15}$$

$$\eta = \frac{1}{2} \sqrt{\bar{T}} (\cosh \gamma - 1) d\bar{w} + \frac{1}{4} \frac{1}{\sqrt{T}} (\partial\gamma)^2 dw \tag{16}$$

and then from a direct computation it follows that

$$A_{fin} = \frac{i}{2} \int_{\tilde{\Sigma}} \omega \wedge \eta \tag{17}$$

where $\tilde{\Sigma}$ denotes the double cover of the sphere defined by $y^2 = T(w)$. Extending the integration from Σ to $\tilde{\Sigma}$ simply involves a factor of 2 since each form is odd under sheet-exchange. An important property of these forms is that they are both closed. The form ω is clearly closed since it is holomorphic, and the closure of η follows from the equations of motion for γ . Notice that (17) would be true for any choice of the dw component of η . The specific coefficient appearing in (16) is necessary for the closure of the form.

Now we would like to apply the Riemann bilinear identity (RBI) to reduce (17) to one-dimensional integrals over cycles on $\tilde{\Sigma}$. There are two caveats in doing this – the singularities in ω and the singularities in η . These issues were resolved in [8], and we follow the approach used there (see [8] for a more detailed treatment and also [9] for a different approach). The basic idea of the RBI is to write one of the forms of the wedge product as an exact form, $\omega = dF$ where $F = \int_{P_0}^P \omega$, which is always possible on a Riemann surface minus some contour, L . In the present case ω has single poles and thus F will have logarithmic cuts which need to be accounted for. A way to side-step this complication is to spread the single poles in ω into a small square-root cuts such that F has only square-root cuts and no singularities. The cost of doing this is that the genus of $\tilde{\Sigma}$ increases, but the upside is that the application of the RBI is simplified. This takes care of the singularities in ω . Now consider the form η which behaves as $\eta \sim (w - z_a)^{-5/2}$ near the zeros of T . The prescription of [8] is to remove the points z_a from the domain by taking L to be the sum of the standard contour for a Riemann surface of genus g and small contours C_a encircling the points z_a . The integrand of (17) can then be written as $d(F\eta)$ (since $d\eta = 0$ on the domain) and then Stokes theorem can be used to reduce the surface integral to a line integral over the usual boundary of the genus g Riemann surface and the contours C_a . The end result is that each boundary C_a contributes a correction of $\pi/12$ to A_{fin} in (17) while the integral over the boundary of $\tilde{\Sigma}$ gives the usual sum over cycles on $\tilde{\Sigma}$ and thus we have[8]

$$A_{fin} = (\text{number of zeros}) \frac{\pi}{12} - \frac{i}{2} \left(\oint_{\gamma_a} \omega \right) I_{ab}^{-1} \left(\oint_{\gamma_b} \eta \right) \tag{18}$$

where $\{\gamma_a\}$ is a complete basis of cycles on $\tilde{\Sigma}$ and I_{ab} is their intersection matrix. For the four-point function there is generically 4 zeros and 4 poles. When we spread the four poles we introduce an additional 4 cuts and thus the surface is genus 5 and there will be 5 a-cycles and 5 b-cycles; that is $\{\gamma_a\} = \{\gamma_{a_1}, \gamma_{b_1}, \gamma_{a_2}, \dots, \gamma_{a_5}, \gamma_{b_5}\}$. The main point is that we have reduced the computation of the surface integral (17) into a sum of 1-dimensional cycle integrals of a closed form. Such integrals are precisely what integrability is good at computing. In the following section we will see how to compute the cycles $\oint_{\gamma_a} \eta$ by exploiting the integrability of (10).

4 The linear problem

To compute the η -cycles appearing in (18) it is useful to consider the linear problem associated with equation (10). Consider a function ψ obeying

$$(\partial + J_w) \psi = 0, \quad (\bar{\partial} + J_{\bar{w}}) \psi = 0 \quad (19)$$

where the components of the connection $J = J_w dw + J_{\bar{w}} d\bar{w}$ are given by

$$J_w = A_w + \frac{1}{\xi} \Phi_w, \quad J_{\bar{w}} = A_{\bar{w}} + \xi \Phi_{\bar{w}} \quad (20)$$

where A and Φ are independent of the spectral parameter ξ and given in terms of γ and T, \bar{T} . We give the explicit forms of A and Φ in appendix A. Note that we will frequently write the spectral parameter as $\xi = e^\theta$.

Compatibility of equations (19) for all ξ is equivalent to the flatness of J , which is satisfied if γ obeys the equation of motion (10) and T (\bar{T}) is purely holomorphic (anti-holomorphic). In the following section we will discuss the relation between the solutions of the (19) and the η -cycles appearing in (18).

4.1 Basic properties

There are a few aspects of the linear problem which will be essential for the following analysis. Let us comment on each of them in turn.

- *Solutions near punctures.* Using (7) and (12) one can show that near the punctures P_a there are two linear-independent solutions of the form (see Appendix A)

$$\hat{\psi}^\pm(w) \equiv (T/\bar{T})^{1/8} e^{\pm \frac{1}{2} \int^w \xi^{-1} \omega + \xi \bar{\omega}} |\pm\rangle \quad (21)$$

$$\sim (w - w_a)^{\pm \frac{1}{4} \Delta_a \xi^{-1} - \frac{1}{4}} (\bar{w} - \bar{w}_a)^{\pm \frac{1}{4} \bar{\Delta}_a \xi + \frac{1}{4}} |\pm\rangle \quad (22)$$

where $|\pm\rangle$ are the eigenvectors of σ^3 . Notice that there is a solution that is exponentially big and one that is exponentially small as one approaches the puncture P_a .⁵

⁵In going from (21) and (22) we have been careless about the branches of ω . In particular, we may choose

- *‘Small’ solutions.* Demanding that a function is both a solution of the linear problem and also small at some puncture P uniquely defines that solution (up to overall normalization). Thus there is a family of ‘small’ solutions s_a each of which is small at puncture P_a . On the other hand, specifying that a solution has the big asymptotic near P does not uniquely determine the solution since one could create another solution obeying the same boundary conditions by adding an arbitrary multiple of s_P .
- \mathbb{Z}_2 *symmetry and ‘big’ solutions.* Even though one cannot uniquely specify a solution by demanding that it has the big asymptotic near P , there is nevertheless a special solution big near P that is uniquely defined. This follows from the \mathbb{Z}_2 symmetry of the connection (20) which is given by

$$UJ(\xi)U^{-1} = J(e^{i\pi}\xi) \quad (23)$$

where $U = i\sigma^3$. This symmetry implies that if $s_P(\xi)$ (we are suppressing the w, \bar{w} dependence) is the solution to (105) small at P then

$$\tilde{s}_P \equiv \sigma^3 s_P(e^{-i\pi}\xi) \quad (24)$$

is another solution of the linear problem. Moreover, from (21) it follows that \tilde{s}_P is *big* at P . Thus we have a second uniquely defined family of solutions \tilde{s}_a , each of which is big at puncture P_a .

- *Products of solutions.* Given two solutions of the linear problem ψ_1 and ψ_2 , there is a natural SL_2 invariant inner product

$$(\psi_1 \wedge \psi_2) \equiv \text{Det} [\{\psi_1, \psi_2\}] \quad (25)$$

This inner product is equivalent to the Wronskian of the two solutions. Important properties of this Wronskian are that it is independent of w and \bar{w} , and thus only depends on the spectral parameter ξ . Further, the product will vanish if the two solutions are linearly *dependent*.

Now that we have introduced these basic facts of the linear problem, we can state what is perhaps the key ingredient in the whole computation.⁶ We claim that the $\xi \rightarrow 0$ expansion of the inner product of two small solutions is the following[10, 8]

$$(s_a \wedge s_b) \sim \exp \left[\frac{1}{2}\xi^{-1}\varpi_{ab} + \frac{1}{2}\xi\bar{\varpi}_{ab} + \xi \int_a^b \eta + \mathcal{O}(\xi^2) \right] \quad (26)$$

a particular branch at some P_a such that the near-puncture solutions take the form (22) but then if we smoothly continue \sqrt{T} to some other puncture P_b it is possible that the small and big solutions correspond to the opposite components from the small and big solutions at P_a . This will be very important below, since it will usually be the case in the construction we will use.

⁶To our knowledge the following fact first appear in [10]. Later it was used in [8, 9] for 3-point function computations. We give a derivation in appendix B; we thank Pedro Vieira and Amit Sever for explaining the basic components of the derivation used for [10]. A different derivation appears in [9].

where η is precisely the same form (16) that appears in the action formula (18) and ϖ_{ab} , $\bar{\varpi}_{ab}$ are explicitly known in terms of integrals of ω and $\bar{\omega}$.⁷ A derivation of (26) is given in appendix B. The point is that by computing the inner products $(s_a \wedge s_b)(\xi)$ we can extract the “puncture-puncture” integrals $\int_a^b \eta$ by extracting the $\mathcal{O}(\xi)$ coefficient of this inner product. All of the η -cycles appearing in (18) can be written in terms of linear combinations of these puncture-puncture integrals. Thus, we can compute area (18) by computing the inner products $(s_a \wedge s_b)$. The rest of this section is devoted to explaining how we compute such inner products using techniques from integrability.

4.2 Defining solutions globally

Let us now comment on how to globally define the small solutions. Suppose that we want to construct the small solution s_P away from puncture P , say at some generic point A . To do this we need to use the connection to transport the solution along some path from the neighborhood of P to the point A . However, it is clear from (21) that the solutions of the linear problem have non-trivial monodromies around the punctures and therefore homotopically different paths on the 4-punctured sphere will result in different values of the small solution at A . In other words, solutions of the linear problem live on a (generically infinite-sheeted) Riemann surface with branch points at the punctures. For the purposes of calculating it is convenient to fix some conventions for dealing with the multivaluedness of the solutions. We first define the sheets by cutting the Riemann surface as shown in figure 5. The cuts all join at a common point and the monodromy about that point is the identity since a path passing through all the cuts is contractable on the sphere. We then define the value of the small solution associated with puncture P at some point A as follows. Draw any curve from the neighborhood of P to A . In the neighborhood of P one starts with s_P . For every time the path crosses a cut emanating from some puncture Q in the *clockwise* (*counterclockwise*) sense attach a factor M_Q (M_Q^{-1}).⁸ In this way, if we transport along a path that is homotopically equivalent to a path that does not cross any cuts then the small solution at A will be $s_P|_A$. If the path crosses the cut emanating from puncture Q once in the clockwise sense, then the value of the small solution at A will be $(M_Q s_P)|_A$, and so on (see figure 5). In the case when s_P is transported around the puncture P one can see from the explicit form (21) of s_P near P that the result will be multiplication by a constant. That is

$$M_P s_P = \mu_P s_P \tag{27}$$

$$M_P \tilde{s}_P = \tilde{\mu}_P \tilde{s}_P \tag{28}$$

⁷To be more precise, this expansion will be true for certain s_a and s_b depending on certain conditions stemming from the form of T and also depending on the value of $\text{Arg}(\xi)$. Furthermore, the contour of integration will be precisely defined by these conditions. We will discuss these conditions in detail below.

⁸Note that the result of a monodromy can be expressed as the linear map M since both s and Ms are solutions of the linear problem. Therefore they can both be expanded in terms of two linearly independent solutions of the linear problem, and thus they are related to each other simply by a linear map, or in other words simply by multiplication by some matrix, M .

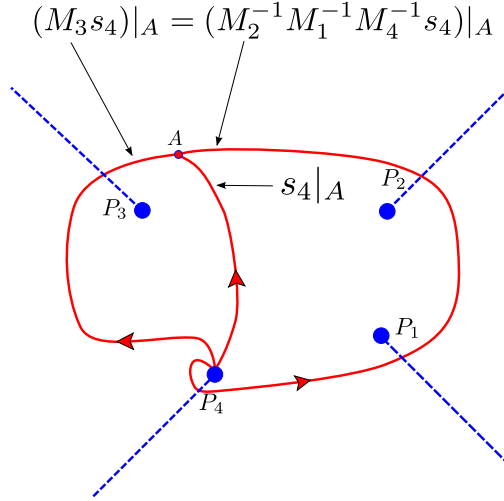


Figure 5: Our conventions for defining the solutions globally. The dashed blue lines emanating from the punctures indicate the conventions for ‘cutting’ the full Riemann surface, thus defining the sheets. The red lines indicate the parallel transport of a solution from P_4 to the point A along three paths. Two of the paths are homotopically equivalent due to the triviality of the total monodromy $M_4 M_3 M_2 M_1 = 1$ (which follows from the fact that any path encircling all the punctures with the same orientation is contractable on the sphere). The third path is homotopically distinct from the other two, and thus the value of the solution at A will differ by monodromy factors.

so that s_P and \tilde{s}_P are eigenvectors of M_P with eigenvalues μ_P and $\tilde{\mu}_P = 1/\mu_P$ respectively. One cannot repeat such an analysis to evaluate $M_Q s_P$ since generically one does not know the explicit form of s_P in the neighborhood of Q .

4.3 WKB approximation and WKB Curves

As we will discuss shortly, it will be essential to have control over the $\xi \rightarrow 0, \infty$ asymptotics of the inner products $(s_P \wedge s_Q)(\xi)$. It is clear from (19)–(20) that these are both singular limits, and the basic idea of extracting this singularity – which is called the *WKB approximation* – is as follows.⁹ As discussed above, we have good control over the solutions in the neighborhood of the punctures. Thus we would like to study, in the limits $\xi \rightarrow 0, \infty$, the transport of small s_P along a curve $w(t)$ which connects a neighborhood of a puncture P with a neighborhood of another puncture Q . Let us consider the transport away from P (see figure 6). We will discuss the $\xi \rightarrow 0$ limit since the $\xi \rightarrow \infty$ limit is similar.

At any point in Σ the matrix Φ has the two eigenvalues $\mp\omega/2 = \mp\sqrt{T}/2 dw$ (which are single valued on the double cover $\tilde{\Sigma}$), and thus we can choose a gauge along $w(t)$ where Φ is diagonal and given by

$$\Phi = \frac{1}{2} \begin{pmatrix} -\omega & 0 \\ 0 & \omega \end{pmatrix} = \frac{1}{2} \begin{pmatrix} -\sqrt{T}dw & 0 \\ 0 & \sqrt{T}dw \end{pmatrix} \quad (29)$$

⁹See appendix B or [12] for a more detailed treatment.

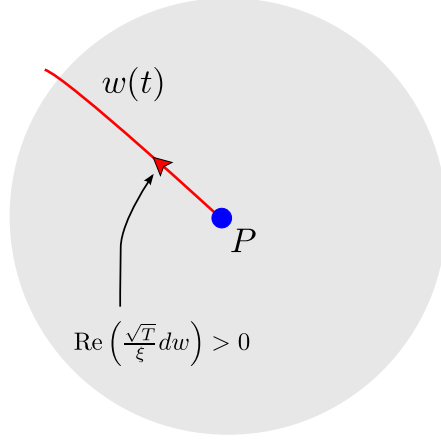


Figure 6: Transporting s_P away from P along $w(t)$. We have chosen the branch of Φ in (29) such that $s_P \propto |+\rangle$ near w_P . In other words, we have chosen the branch of Φ such that $\text{Re}(\langle + | -\Phi_w/\xi dw | + \rangle) = \text{Re}(dw\sqrt{T}/\xi) > 0$ for dw pointing along $w(t)$ away from P and thus $\exp\left(\int_{w'_P}^{w(t)} dw\sqrt{T}/\xi\right)$ is exponentially diverging as $\xi \rightarrow 0$.

In the limit $\xi \rightarrow 0$ some component of Φ/ξ will dominate and thus the leading contribution to s_a at some point w along $w(t)$ will be given by

$$e^{-\int_{w'_a}^w \Phi/\xi} |\sigma\rangle \quad (30)$$

where the value of $\sigma = \pm$ depends on the branch of Φ we have chosen (recall that $|\pm\rangle$ are the eigenvectors of σ^3). This is the singular contribution in the limit $\xi \rightarrow 0$ for the same reason that it is the small solution – namely, because

$$\text{Re}(\langle \sigma | (-\Phi/\xi) | \sigma \rangle) > 0 \quad (31)$$

along a path traveling away from P_a . The basic statement of the WKB approximation is that so long as we transport along paths such that (31) is true along the whole path then the leading contribution to s_P in the $\xi \rightarrow 0$ limit is indeed given by (30). In other words, as long as we transport along curves satisfying (31) everywhere, then we can reliably extract the singularity as $\xi \rightarrow 0$ as it is simply given by (30). The curves along which (31) is satisfied most strongly are those for which

$$\text{Im}(\langle \sigma | (-\Phi/\xi) | \sigma \rangle) = 0 \quad (32)$$

Curves satisfying this condition are called *WKB curves*. If we transport along some curve satisfying (32) for $\text{Arg}(\xi) = \phi$, then the condition (31) will be satisfied for $\text{Arg}(\xi) \in (\phi - \pi/2, \phi + \pi/2)$. In fact, we will need to control the asymptotics of s_P in precisely such a wedge of the ξ -plane, and thus we should always transport along WKB lines. We will give the a very brief overview of the properties of these lines in the next subsection. For a detailed treatment see [12].

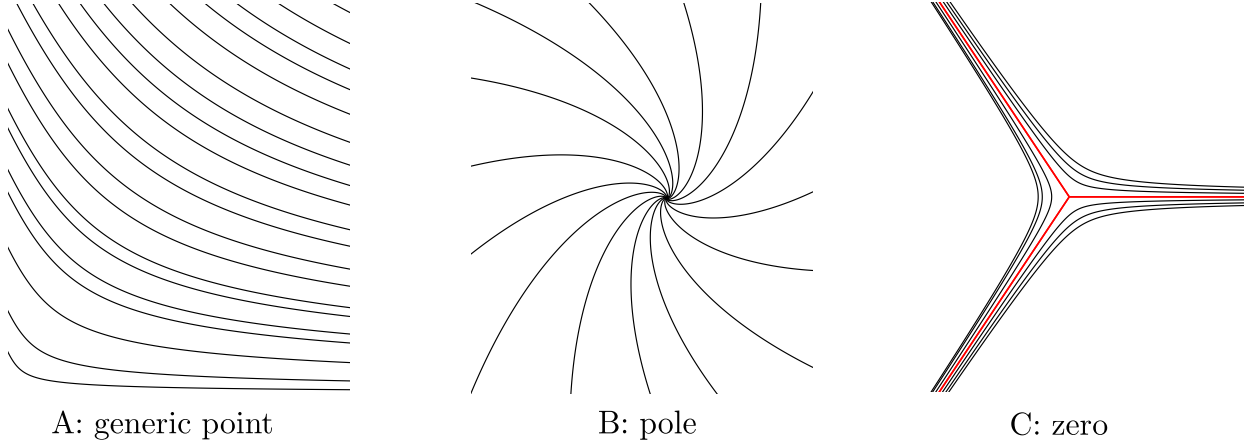


Figure 7: Local structure of WKB lines in the neighborhood of, A: a generic point; B: a double pole of T ; C: a simple zero of T . In the case of a generic point the WKB curves form continuous non-intersecting lines. In the case of a singular point they form logarithmic spirals for generic values of $\text{Arg}(\xi)$. The exact nature of these spirals will not be important. What is important is that the singular points act as sources/sinks of WKB curves. In the case of a zero, there are three special WKB curves that asymptote to the zero which are the red curves in panel C . These special curves, called separating curves, determine the global structure of the WKB foliation.

4.4 WKB triangulation

As we discussed in section 4.2 we define the solutions of (19) globally by transporting along specific paths. Transport of solutions along homotopically equivalent paths will lead to the same result, whereas transport along homotopically inequivalent paths generically will give different results. For this reason it is useful to set up a system of fiducial paths between the punctures which we will use to globally define the solutions. Because we will need to control the large/small ξ asymptotics of the Wronskians, it is best to choose these paths to be WKB curves – i.e. curves satisfying (32).

We will first consider the local structure of WKB curves. In the neighborhood of a generic point on the punctured sphere the WKB curves are smooth and non-intersecting (see figure 7A). In the neighborhood of a (double) pole of T the WKB curves follow logarithmic spirals that asymptote to the singular point (see figure 7B). All that will be important here is that the poles act as sources/sinks of WKB curves but the exact nature of these spirals will not be important. Finally, working in the neighborhood of a simple zero of T one can show that there are three special WKB curves that asymptote to the zero and which govern the WKB lines near the zero (see figure 7C).

Now consider the global structure of the WKB curves. All WKB curves fall into one of the following types [12]

- *Generic WKB curves* which are those that asymptote in both directions to a pole of T (potentially the same one);
- *Separating WKB curves* which asymptote to a zero of T in one direction and to a pole

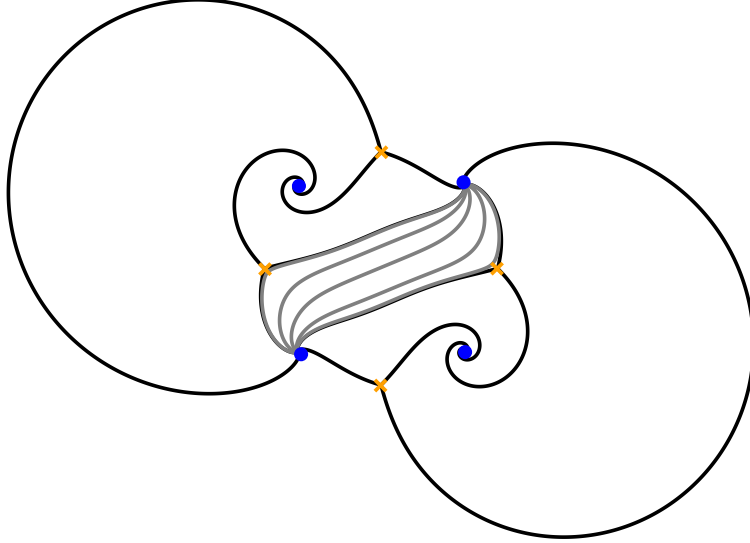


Figure 8: Global WKB structure for an example with 4 punctures. The separating curves are shown in black. In one cell we show several examples of homotopically equivalent curves (shown in gray) that sweep the cell. Each cell defined by the separating curves has a 1-parameter family of such curves. By choosing a representative curve from each family we obtain the triangulation shown in figure 9. Notice that near each puncture (the blue dots) we see the spiral structure shown in panel B of figure 7 and near each zero (yellow \times) we see the local structure shown in panel C of figure 7.

of T in the other;

- *Finite WKB curves* which are closed or asymptote in both directions to a zero of T (potentially the same one).

We will now describe how we use the WKB curves to set up a system of fiducial paths, or more specifically, a *triangulation*. By triangulation we mean a triangulation of the punctured sphere with all vertices at the punctures and at least one edge incident on each vertex. Consider fixed T and $\text{Arg}(\xi)$ such that there are no finite WKB curves (this can always be done since such curves only appear at special, discrete values of $\text{Arg}(\xi)$). First draw all of the separating WKB curves – there will be $3N_Z$ of these, where N_Z is the number of zeros of T (since for the moment we are not allowing finite WKB curves). These curves will divide the punctured sphere up into cells with each cell defining a family of homotopically equivalent *generic* WKB curves as shown in figure 8 for an example of the 4-punctured sphere. To construct the triangulation, choose a representative curve from each cell, e.g. any one of the silver curves shown in figure 8. The claim is that the collection of these representative curves, which we will call *edges*, gives the desired triangulation [12].¹⁰ As a concrete example, the triangulation associated with the cell-construction of figure 8 is shown in figure 9. This same triangulation will play an important role in the 4-point function computation below.

¹⁰To see this in general consider a single zero of T as shown in figure 7. The zero is on the boundary of three cells. Choosing edges from the family of curves in each cell we see that they form a triangle. Thus the edges form a triangulation of the punctured sphere with each triangle containing a zero of T .

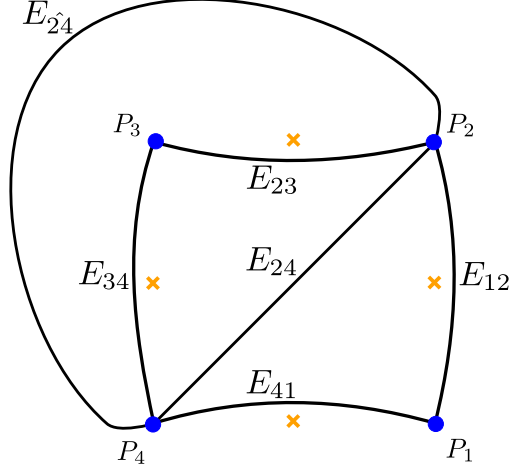


Figure 9: The WKB triangulation of the 4-punctured sphere following from the WKB foliation shown in figure 8. Each edge E_{ab} of the triangulation is a representative from one of the families of homotopically equivalent lines in each cell of figure 8. This triangulation will be of central interest in the 4-point function computation.

We have now finished the discussion of how to construct the WKB triangulation for a given T and $\text{Arg}(\xi)$. Before moving on to the next section let us discuss one final point. In the following it will be useful to lift edges of the triangulation to the double cover $\tilde{\Sigma}$ and to endow the lifted edges with an orientation. Recall that $\omega = \sqrt{T}dw$ is a single valued form on $\tilde{\Sigma}$. Let ∂_t be a tangent vector of the lifted edge E at a point on $\tilde{\Sigma}$. There are of course two possible orientations for ∂_t . Note that by virtue of (32) we have $e^{-i\phi}\omega \cdot \partial_t \in \mathbb{R}$. We define the orientation of the lifted edge E by the condition $e^{-i\phi}\omega \cdot \partial_t > 0$. Notice that each edge on the punctured sphere will lift to two edges – one on each sheet of $\tilde{\Sigma}$ and that these two edges will have opposite relative orientation. Picking a particular orientation of some edge is equivalent to picking a particular sheet of $\tilde{\Sigma}$.

4.5 Coordinates

From the WKB triangulation we will now construct the so-called Fock-Goncharov coordinates [12]. These are natural objects to work with because they are gauge invariant and independent of the normalization of the small solutions. From the coordinates we will be able to extract the η -cycles that we need to compute the action (18).

Consider some edge E of the triangulation. This edge is shared by precisely two triangles, and these triangles form the quadrilateral Q_E (see figure 10). Number the vertices of Q_E as shown in figure 10 with E going between P_1 and P_3 . As we mentioned in section 4.1, associated with each puncture P_a there is a small solution s_a . The solutions cannot be made globally smooth and single valued on the punctured sphere due to the monodromy around each puncture. However, we can define them such that they are single valued and smooth

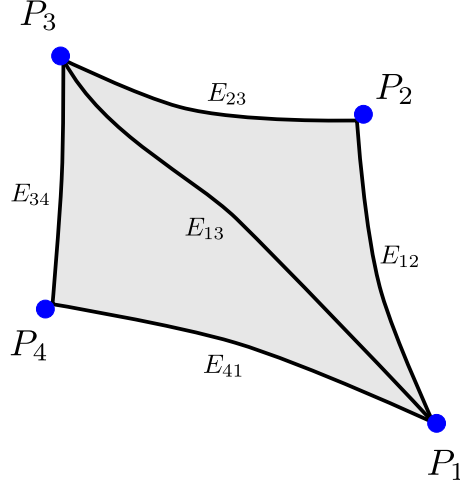


Figure 10: The two triangles sharing the edge E_{13} . These two triangles define the quadrilateral $Q_{E_{13}}$, which is shown in gray shading. Each blue dot represents a puncture, which are the vertices of the triangulation and each black line and is an edge.

throughout Q_E .¹¹ We then define the Fock-Goncharov coordinate as [12]

$$\chi_E = (-1) \frac{(s_1 \wedge s_2)(s_3 \wedge s_4)}{(s_2 \wedge s_3)(s_4 \wedge s_1)} \quad (33)$$

where all the s_a are evaluated at a common point in Q_E .

As a concrete example consider the triangulation of the 4-punctured sphere shown in figure 9. In figure 11 we show how to apply the procedure just described to construct the coordinates corresponding to edges E_{24} and $E_{\hat{2}4}$. Consider first the left panel of 11. We define each solution s_a throughout Q_{24} by parallel transporting from each P_a where the explicit form of the solutions is known – see (21). The red lines indicate the parallel transport of each s_a from P_a to a common point A ; clearly we can define the small solutions at any point $A \in Q_{24}$ in this way. Further, if the paths never leave the quadrilateral (or at least is always homotopically equivalent to a paths that never leave the quadrilateral) then the solution defined in this way is guaranteed to be single-valued and smooth throughout the quadrilateral, as required. With the solutions defined at a common point in the quadrilateral we can construct the coordinate χ_{24} , which is independent of the choice of $A \in Q_{24}$. Now consider the right panel of figure 11 where the grey shading indicates the quadrilateral associated to edge $Q_{\hat{2}4}$. These figures should be imagined on the sphere. Now to transport the small solutions to a common point one cannot avoid passing under a cut onto new sheets of some of the small solutions. For example s_2 must pass onto a new sheet in order to be smoothly continued to the point A . This is because if we were to compare the s_2 of the left panel and the s_2 of the right panel (by moving each respective A to a common point A' along the edge E_{34} , for example) the two paths of continuation would differ by a holonomy around P_3 , and thus the values at the point A' would not coincide but would differ by the action

¹¹We will show this in some concrete examples momentarily.

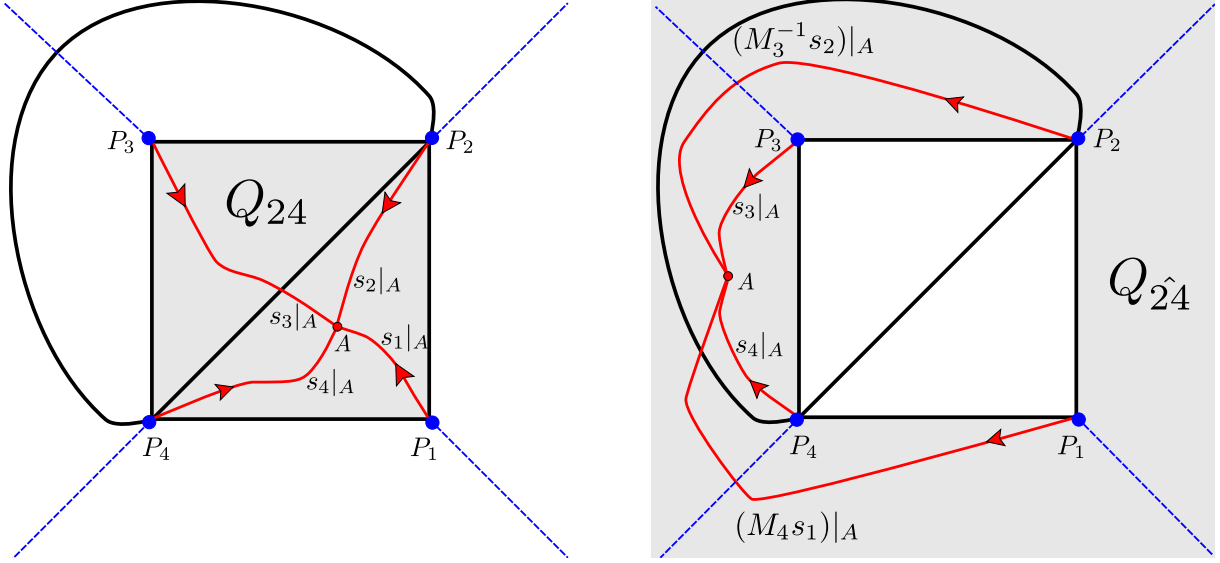


Figure 11: Here we show how to construct the coordinates χ_{24} (left panel) and $\chi_{\hat{2}4}$ (right panel) of the triangulation of figure 9. The gray shaded regions represent Q_{24} and $Q_{\hat{2}4}$ respectively. These figures should be pictured on the sphere. The dashed blue lines emanating from the punctures indicate our conventions for defining the sheets of the small solutions as explained in section 4.2. The red lines indicate how we globally define the solutions s_a by transporting away from P_a using the connection. We use paths that never leave the quadrilateral such that the solutions used to form the coordinates are guaranteed to be single-valued and smooth throughout the quadrilateral, as required.

of $M_3^{\pm 1}$. Of course which solution we call s_2 and $M_3^{\pm 1}s_2$ is purely a matter of convention. Similarly, which solutions acquire factors of M_a depends on the choice of the point A . We stress that the coordinates are independent of all such ambiguities, as one can easily check using identities such as $(M_c s_a \wedge s_b) = (s_a \wedge M_c^{-1} s_b)$, etc. Then from figure 11 we read off

$$\chi_{24} = (-1) \frac{(s_2 \wedge s_3)(s_4 \wedge s_1)}{(s_3 \wedge s_4)(s_1 \wedge s_2)}, \quad \chi_{\hat{2}4} = (-1) \frac{(M_3^{-1} s_2 \wedge M_4 s_1)(s_4 \wedge s_3)}{(M_4 s_1 \wedge s_4)(s_3 \wedge M_3^{-1} s_2)}. \quad (34)$$

We will also need to construct coordinates in the slightly degenerate case where the coordinate corresponds to an edge ending at a vertex that has only two incident edges (including the edge under consideration) for example all edges in figure 9 except E_{24} and $E_{\hat{2}4}$. We show how to construct this coordinate in figure 12. Using the procedure described there we find

$$\chi_{23} = (-1) \frac{(s_2 \wedge M_3 s_4)(s_3 \wedge s_4)}{(M_3 s_4 \wedge s_3)(s_4 \wedge s_2)}, \quad \chi_{12} = (-1) \frac{(s_1 \wedge M_1^{-1} s_4)(s_2 \wedge s_4)}{(M_1^{-1} s_4 \wedge s_2)(s_4 \wedge s_1)} \quad (35)$$

The other two coordinates χ_{34} and χ_{14} are computed in a similar way.

We have now completed our discussion of how to construct the coordinates. Before we continue, let us comment on a useful property of these objects. Consider multiplying all of the coordinates associated with edges meeting a given puncture P . For example, the edges

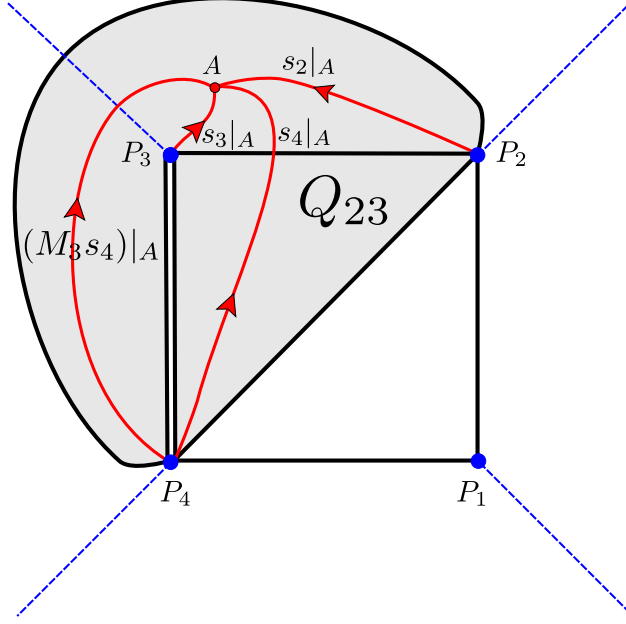


Figure 12: Here we describe the construction of the coordinate for the slightly degenerate case where the coordinate corresponds to an edge ending at a vertex that has only two incident edges (e.g. P_2 has only 2 incident edges: E_{12} and E_{23}). We construct the coordinate for edge E_{23} of the triangulation shown in figure 9. The quadrilateral prescription described above still applies, but one must take care to correctly define Q_E and the solutions inside Q_E . First of all, in order to have single-valued and smooth solutions throughout Q_{23} we must exclude a region between P_3 and P_4 . Otherwise Q_{23} would contain P_3 and thus the solutions could not be single valued in Q_{23} (there would be a monodromy around P_3). Since the boundaries of the quadrilateral must be edges of the triangulation, the only choice is to remove a thin region running along edge E_{34} and then to treat the two ‘sides’ of E_{34} as different edges. In the figure we have represented this process by showing E_{34} as doubled and with the region between the new edges excluded from Q_{23} . We then define the solutions throughout Q_{23} in the same way as described in figure 11, by analytically continuing the solutions along paths from P_a to A that stay within Q_{23} which is represented as the shaded region. Once we have defined the solutions at a common point we form the coordinate χ_{23} given in equation (35).

ending at P_2 in the triangulation of figure 9 are E_{12} , E_{24} , E_{23} and E_{24} . Using (34)-(35) we have

$$\chi_{12}\chi_{24}\chi_{23}\chi_{24} = \mu_2^2. \quad (36)$$

This property is true in general since the inner-products in the coordinates telescopically cancel in the product and the only thing that remains is the effect of the monodromy around the puncture which produces a μ_P^2 factor. Thus we have the general rule [12]

$$\prod_{E \text{ meeting } P} \chi_E = \mu_P^2. \quad (37)$$

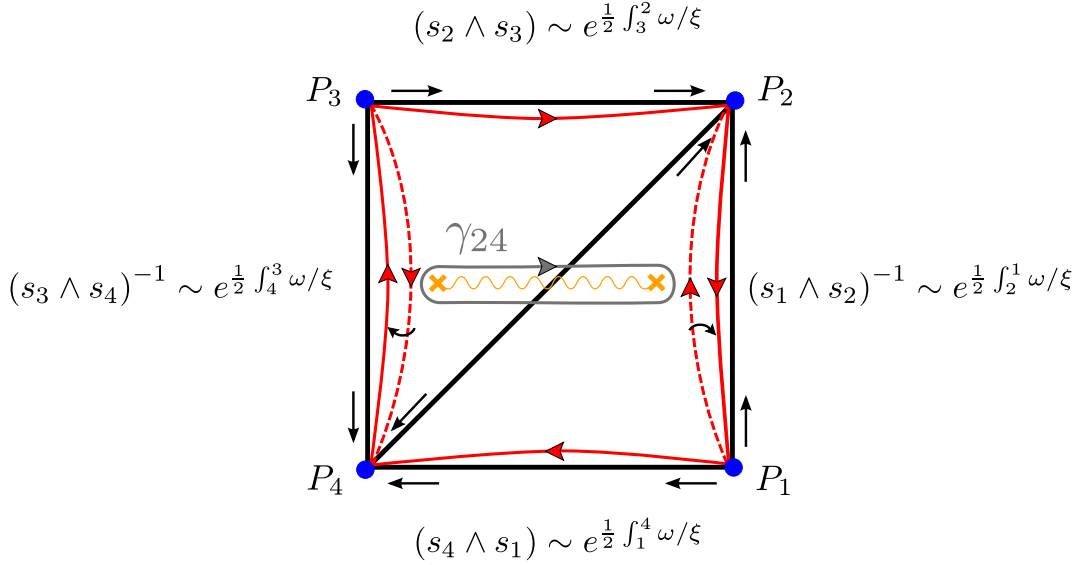


Figure 13: Computing the $\xi \rightarrow 0$ asymptotic of the coordinate χ_{24} for a typical WKB triangulation. The blue disks represent the punctures and the black lines represent edges of the triangulation. A yellow \times represents a zero of ω and the wavy yellow line shows our convention for defining the sheets of $\tilde{\Sigma}$. The black arrows running along the edges indicate the choice of the direction for the edges. Each red curve indicates the transport of a small solutions in the limit $\xi \rightarrow 0$. The dashed red lines correspond to the transport of a solution appearing in the *denominator* of the coordinate. The transports used to form the coordinate combine into the continuous integral of ω near the boundary of Q_{24} , which can then be deformed into the cycle integral γ_{24} shown in gray.

4.6 WKB asymptotics of the coordinates

The advantage of using the WKB triangulation is that the $\xi \rightarrow 0, \infty$ asymptotics of the coordinates of the triangulation are easily extracted given the discussion of section 4.3. That is, because we have maximum control over the large/small ξ asymptotics of the small solutions when we transport along WKB curves. We give only the basic idea of the derivation of these asymptotics here and refer the reader to appendix B and [12] for details.

To obtain the asymptotic of some χ_E one simply needs to use expression (30) for each inner-product of the coordinate, taking care to account for the direction of the WKB lines. Consider the coordinate associated with edge E_{24} in figure 13. The expression for this coordinate in terms of the small solutions is given in (34). We will now use formula (30) to compute the asymptotic of this coordinate in the $\xi \rightarrow 0$ limit. Let us take the directions of the WKB lines to be as given in figure 13. To evaluate the inner product $(s_2 \wedge s_3)$ we must transport the solutions to a common point. Since there is a WKB line flowing from P_3 to P_2 we can safely use (to leading order) expression (30) to transport s_3 to the neighborhood of P_2 , giving a contribution of the form $(s_2 \wedge s_3) \sim e^{\frac{1}{2}} \int_{s_3}^2 \omega / \xi$. To evaluate $(s_3 \wedge s_4)$ we must transport s_3 to P_4 since that is the direction of the WKB line and thus we get the contribution $(s_3 \wedge s_4) \sim e^{\frac{1}{2}} \int_{s_3}^4 \omega / \xi$. We may then reverse the order of integration in $(s_3 \wedge s_4)$ and also move it to the numerator of the coordinate. Then the integrations from $(s_2 \wedge s_3)$ and $(s_3 \wedge s_4)$

combine nicely into a continuous integral running just inside the boundary of Q_{24} from the neighborhood of P_2 to P_3 to P_4 . Repeating this analysis for the remaining two brackets one obtains a closed cycle integral passing along the boundary of Q_{24} . Recall from the discussion of section 4.4 that each triangle in the WKB triangulation encloses one zero of ω . The integral of ω thus encloses two zeros and so it can be deformed to the cycle integral shown in figure 13. Thus the non-vanishing contribution in the limit $\xi \rightarrow 0$ is given by

$$\chi_E \sim (-1) \exp \left(\frac{1}{2} \xi^{-1} \int_{\gamma_E} \omega + C_E^{(0)} \right) \quad (38)$$

The contour γ_E is the cycle encircling the two zeros contained in Q_E and its direction is the same as that of the WKB lines corresponding to the brackets in the numerator of the coordinate. The term $C_E^{(0)}$ is the $\mathcal{O}(\xi^0)$ contribution to the WKB expansion, which we will discuss momentarily. The overall (-1) prefactor in (38) is the same (-1) appearing in the definition of the coordinate (33).

To derive the subleading WKB corrections (in the $\xi \rightarrow 0$ limit, for example) is essentially a matter of perturbation theory once the singular contribution has been extracted. We give a detailed discussion of this in appendix B. Here we will simply focus on the result and its implications. We find the first subleading contribution is given by

$$C_E^{(0)} = \log(-1)^{u_E} \pm i\pi \quad (39)$$

where u_E is the number of u -spikes enclosed by γ_E .

Finally the $\xi \rightarrow \infty$ asymptotic follows in the same way as the $\xi \rightarrow 0$ and leads to a cycle integral around Q_E of $\xi\bar{\omega}$.

To summarize, the $\xi \rightarrow 0, \infty$ asymptotics for χ_E are given by

$$\chi_E \sim (-1)^{u_E} \exp \left[\frac{1}{2} \int_{\gamma_E} (\xi^{-1}\omega + \xi\bar{\omega}) \right] \quad (40)$$

where γ_E is the cycle encircling the two zeros contained in Q_E and its direction is the same as that of the WKB lines corresponding to the brackets in the numerator of the coordinate. Now it is clear how the choice of spikes (i.e. the choice of signs in (11)) is encoded into the coordinates – via the constant term in the WKB expansion which contributes the $(-1)^{u_E}$ factor in (40). Recall that u_E is the number of u -spikes encircled by γ_E .

4.7 Shift relation.

In section 4.1 we explained that there are two special solutions s_P, \tilde{s}_P associated with each puncture P and that they are related to each other by a shift in the spectral parameter: $\tilde{s}_P(\xi) = \sigma^3 s_P(e^{-i\pi}\xi)$. Here we give an alternative relation between the small and big solutions that does not involve shifting the spectral parameter. The solutions s_P and \tilde{s}_P are linearly independent and thus we can expand any solution s_Q in terms of them. In particular we

have

$$s_Q = \left(\frac{\tilde{s}_P \wedge s_Q}{\tilde{s}_P \wedge s_P} \right) s_P + \left(\frac{s_P \wedge s_Q}{s_P \wedge \tilde{s}_P} \right) \tilde{s}_P \quad (41)$$

$$M_P s_Q = \left(\frac{\tilde{s}_P \wedge s_Q}{\tilde{s}_P \wedge s_P} \right) \mu_P s_P + \left(\frac{s_P \wedge s_Q}{s_P \wedge \tilde{s}_P} \right) \mu_P^{-1} \tilde{s}_P \quad (42)$$

For the second equality we have used (27)-(28). Combining these two equations it follows that

$$\left(\frac{M_P s_Q \wedge s_Q}{M_P s_Q \wedge s_P} \right) = (1 - \mu_P^2) \left(\frac{\tilde{s}_P \wedge s_Q}{\tilde{s}_P \wedge s_P} \right) \quad (43)$$

The utility of this equation is that it allows us to replace certain wronskians involving big solutions (as on the RHS of (43)) in terms of small solutions with monodromies. This will play a key role in the derivation of the functional equations that we present in the following section.

4.8 χ -system.

We will now derive a set of functional equations for the coordinates which, together with certain analytic properties, allows us to determine the coordinates completely. Our inspiration comes from the solution of the bosonic Wilson-loop problem at strong coupling [10] where the solution involves a set of functional equations of the schematic form¹²

$$Y_a^+ Y_a^- = F_a(Y) \quad (44)$$

where $f^{n \times \pm} \equiv f(\theta \pm ni\pi/2)$. On the RHS of (44) the function F_a can depend on all of the Y_a , but with their arguments un-shifted. The only shifts in the spectral parameter occur on the LHS of (44). For the Wilson-loop problem the F_a are such that (44) takes the form of a so-called Y-system which commonly appear in the context of 1+1 dimensional integrable QFT's. Here, using the general formalism of [12], we will arrive at a set of functional equations with the same schematic form as (44) but with the F_a of a different form than that occurring in the Wilson-loop problem. We will call this type of functional equation a χ -system.

To derive a relation of the form (44) we begin with the LHS. Using (24) we have

$$\chi_E \tilde{\chi}_E = \chi_E \chi_E^{++} \quad (45)$$

where $\tilde{\chi}_E$ is defined by taking χ_E and replacing each small solutions $s_a \rightarrow \tilde{s}_a$. To obtain the schematic form (44) we need to rewrite (45) in terms of only un-shifted small solutions. That is, we need to get rid of all the tildes without introducing any shifts in the spectral parameter. For this we can use (43) after applying the Schouten identity¹³ to (45) to obtain

$$\chi_E \chi_E^{++} = \chi_E \tilde{\chi}_E = \frac{(1 + A_{ab})(1 + A_{cd})}{(1 + A_{bc})(1 + A_{da})} \quad (46)$$

¹²The linear problem associated with that problem is very similar to the one considered here and the Y_a are (up to shifts in the spectral parameter) the coordinates associated with that problem. We are referring here to the special case where the Wilson loop lives in an $\mathbb{R}_{1,1}$ subspace.

¹³ $(s_a \wedge s_b)(s_c \wedge s_d) + (s_a \wedge s_c)(s_d \wedge s_b) + (s_a \wedge s_d)(s_b \wedge s_c) = 0$.

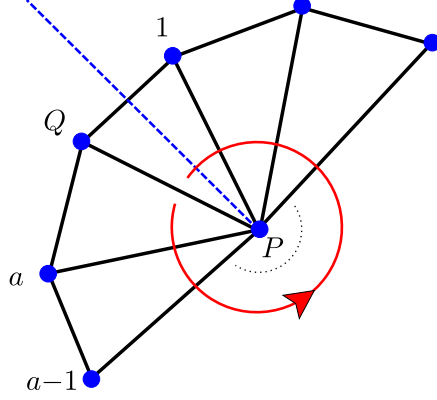


Figure 14: Graphical rules for constructing $\Sigma(P; Q \rightarrow Q)$. Start at edge E_{PQ} and continue in a *counterclockwise* fashion about P forming the nested product (49) by multiplying the coordinates for each edge encountered along the way (i.e. the coordinates associated with each edge intersected by the red line in the order indicated by the arrow). The dashed blue line indicates our convention for cutting the solutions to account for the monodromy around P . The small solutions used to form the coordinates are defined in the vicinity of P by analytically continuing them throughout the triangles along the direction indicated by the red arrow and thus if we use s_Q in $\chi_{P,a}$ then we must include a monodromy matrix when the solution is continued around P to form $\chi_{P,1}$.

where we have defined the useful auxiliary quantity

$$A_{PQ} = (-1) \frac{(s_Q \wedge \tilde{s}_P)(s_P \wedge \tilde{s}_Q)}{(s_P \wedge \tilde{s}_P)(s_Q \wedge \tilde{s}_Q)} \quad (47)$$

$$= (-1) (1 + \mu_P^2)^{-1} (1 + \mu_Q^2)^{-1} \left(\frac{M_{PSQ} \wedge s_Q}{M_{PSQ} \wedge s_P} \right) \left(\frac{M_{QSP} \wedge s_P}{M_{QSP} \wedge s_Q} \right) \quad (48)$$

Here, the edge E is the edge ac in Q_E where the vertices are labeled $abcd$ in counter-clockwise order. To go from (47) to (48) we used the shift relation (43). The last step is to rewrite the wronskians appearing in (48) in terms of the coordinates. Once this is done, combining (45) – (48), we can assemble a functional equation of the form (44). To do this (following [12]) we introduce the quantity

$$\Sigma(P; Q \rightarrow Q) = 1 + \chi_{P,a} (1 + \chi_{P,a-1} (1 + \dots \chi_{P,2} (1 + \chi_{P,1}))) \quad (49)$$

The coordinates appearing in this object are shown in figure 14. By repeatedly applying the Schouten identity (see footnote 13) starting with $(1 + \chi_{P,1})$ one can see that the Wronskians in (49) telescopically cancel so that¹⁴

$$\Sigma(P; Q \rightarrow Q) = \frac{(s_0 \wedge s_{a+1})(s_P \wedge s_a)}{(s_{a+1} \wedge s_a)(s_0 \wedge s_P)} = \frac{(s_P \wedge s_a)(M_{PSQ} \wedge s_Q)}{(s_Q \wedge s_a)(M_{PSQ} \wedge s_P)} \quad (50)$$

¹⁴An easy way to see this in general is to use induction [12]. The case $a = 1$ is simple to prove using Schouten identity. Then one can show (again using Schouten) that $\Sigma(P; Q_{a+2} \rightarrow Q_0) = 1 + \chi_{P,a+1} \Sigma(P; Q_{a+1} \rightarrow Q_0)$.

In going from the first equality to the second in (50) we have accounted for the monodromy acquired by the small solutions when they are analytically continued around P (see figure 14). Then, from (50) and (48) we have

$$(1 + \mu_P)^2(1 + \mu_Q)^2 A_{PQ} = \chi_{PQ} \Sigma(P; Q \rightarrow Q) \Sigma(Q; P \rightarrow P) \quad (51)$$

Finally, using (51) in (46) and noting (49) we obtain a closed functional equation for χ_E of the form (44). Repeating this procedure for the coordinate associated to each edge in a given triangulation gives the desired set of functional equations. Note that this procedure can be applied to derive the χ -system for an arbitrary number of punctures. In section 5 we will apply this procedure to the triangulation (9), which is one of the triangulations of interest for the four-point function computation.

4.9 Inverting χ -systems

In the previous section we showed how to derive the χ -system associated with a given triangulation of the N -punctured sphere. In this section we will discuss how to use the χ -system along with certain analytic properties of the coordinates to obtain integral equations that determine the χ_E uniquely.

The basic idea behind the inversion of a χ -system is to Fourier transform (the log of) each equation since in Fourier space these nonlocal relations become local as the shifts in the parameter θ can be undone in the usual way. For such a procedure to be successful one must have a certain amount of control of the analytic properties of the coordinates. Let us discuss this carefully. The equations that we want to Fourier transform have the form

$$\log \chi_E^-(\theta + i\phi) + \log \chi_E^+(\theta + i\phi) = \log F_E(\chi^\pm(\theta + i\phi)) \quad (52)$$

where $F_E(\chi)$ is an explicit function of the coordinates which follows from the discussion of section 4.8. We have introduced the arbitrary shift ϕ for reasons that will be explained momentarily. Note that $\chi_E \chi_E^{++} = \chi_E \chi_E^{--}$ since the small solutions are $2\pi i$ -periodic, which is why we can have either shift $F_E(\chi^\pm)$ on the RHS. The choice of this shift is arbitrary since the objects we will eventually compute (the η -cycles) are functionals of the coordinates only through A_{PQ} which is $i\pi$ -periodic and thus does not care about the choice of shift. As a convention we choose the shift $-i\pi/2$.

To Fourier transform the relationship (52) one must be sure that the transform converges. Moreover, to undo the shifts on the LHS, one must account for the singularities (if any) of $\log \chi_E$ in the strip of width π centered along the line where the transform has been performed. We will now discuss each of these issues in turn.

The information from the WKB analysis will allow us to ensure the convergence of the Fourier transform, provided certain conditions are satisfied. First consider the LHS of (52). We need to ensure that the transform of each *individual* term converges. We can ensure this if we know the asymptotics of the coordinates in the full strip $\text{Im}(\theta) \in (\phi - \pi/2, \phi + \pi/2)$. The coordinates should be derived from the triangulation that one has at $\text{Im}(\theta) = \phi$. Then the WKB analysis guarantees that the asymptotics are given by (40) in a strip that includes the region $\text{Im} \in (\phi - \pi/2, \phi + \pi/2)$. Each term on the LHS can be made safe to transform

by making (on the LHS only) the replacement $\chi_E \rightarrow \chi_E/\chi_E^{(0)}$ where $\chi_E^{(0)}$ is the asymptotic (40). This replacement does not modify the equation since $(\chi_E^{(0)}) (\chi_E^{(0)})^{++} = 1$.

Now consider the RHS of (52), which has the form (see equation (46))

$$\log F_E (\chi^\pm (\theta + i\phi)) = \log \left[\frac{(1 + A_{ab})(1 + A_{cd})}{(1 + A_{bc})(1 + A_{da})} (\theta \pm i\pi/2 + i\phi) \right] \quad (53)$$

Each A_{PQ} is computed by (51) and (49). For the RHS of (53) to be decaying it is sufficient for all of the A_{PQ} in (53) to be decaying. If all the χ -functions are decaying then from (51) and (49) it is clear that all of the A_{PQ} will decay; the μ -factors will decay by virtue of the rule (37). On the other hand, if all the χ -functions are growing the μ -factors in (51) will dominate the RHS of (51) so that A_{PQ} is still decaying; to see this one should re-express the μ -factors in terms of the coordinates using (37). Thus the RHS of (53) will decay if all of the χ -functions are growing, or alternatively if they are all decaying. For generic ϕ it will generally not be true that the RHS of (53) is well behaved, and one must try to find a range of ϕ -values for which the χ_E are all decaying or are all growing. If a suitable ϕ can be found, then (52) can be directly solved by Fourier-transform. In all of the examples we have considered (in particular, those relevant for the 4-point function) it has been possible to find such a ϕ .

Concerning the issue of singularities within the strip of inversion, it follows from (19) that the Wronskians $(s_a \wedge s_b) (\theta)$ are (in an appropriate normalization) analytic away from $\theta = \pm\infty$. It is, however, possible for these objects to have *zeros* and in the following it is an assumption that there are no zeros in the strip where we do the inversion.¹⁵ In section 5.1.4 we perform numerical tests that support this assumption.

Finally, we use the Fourier analysis to obtain

$$\log X_E (\theta) = \log X_E^{(0)} (\theta) - \int_{\mathbb{R}} \frac{d\theta'}{2\pi i} \frac{\log F_E (X (\theta'))}{\sinh (\theta' - \theta + i0)} \quad (54)$$

where $X_E (\theta) = \chi_E (\theta + i\phi - i\pi/2)$ and $X_E^{(0)}$ is the (shifted) asymptotic (40) and $F_E (X)$ is an explicit function of the coordinates which follows from the discussion of the previous section.

The equations (54) can easily be solved for the X_E by iterating them in a computer. In the next subsection we will show how to extract the η -cycles of formula (18) from the X_E which are computed using (54). We will then perform some numerical tests in section 5.1.4.

4.10 Extracting η -cycles

Once the coordinates are computed according to the prescription of the preceding section we extract the η -cycles as follows. What we need to compute are the individual Wronskians

¹⁵ In the limit where the WKB approximation holds, i.e. when $\theta \rightarrow \pm\infty$ or in the limit of large zero modes $|Z_E| \rightarrow \infty$ [12], it is clear that (in an appropriate normalization) the Wronskians will not have any zeros since (suppose we compute the Wronskian near P_b) then s_a will be the *big* solution near P_b and is thus linearly independent of s_b which is small at P_b . For finite values of θ (or alternately of $|Z_E|$) we have no concrete way of arguing that these zeros are not present.

$(s_a \wedge s_b)$. For this, note that from (47) and footnote 13 we have

$$(1 + A_{ab}) = \frac{(s_a \wedge s_b)(\tilde{s}_a \wedge \tilde{s}_b)}{(s_a \wedge \tilde{s}_a)(s_b \wedge \tilde{s}_b)} \quad (55)$$

We can choose a gauge where $(s_P \wedge \tilde{s}_P) = 1$. The final result will be gauge independent. With this gauge choice we have

$$\log(s_a \wedge s_b)^- + \log(s_a \wedge s_b)^+ = \log(1 + A_{ab}^-) \quad (56)$$

Here we will use the notation $\theta \rightarrow \theta + i\phi$ where θ and ϕ are real. We then insert the zero-modes on the LHS in the same way as for the χ -system (see section 4.9). We are only interested in P_a and P_b that are connected by a WKB line when $\text{Arg}(\xi) = \phi$, and thus we have good control over the asymptotics in the required strip. Performing the Fourier transforms we obtain

$$\log(s_a \wedge s_b)(\theta + i\phi) = \left(\frac{1}{2} e^{-\theta - i\phi} \varpi_{ab} + \frac{1}{2} e^{\theta + i\phi} \bar{\varpi}_{ab} \right) + \int_{\mathbb{R}} \frac{d\theta' \log(1 + A_{ab}^-(\theta' + i\phi))}{2\pi \cosh(\theta - \theta')} \quad (57)$$

where we have defined

$$\varpi_{ab} \equiv \lim_{w'_a \rightarrow w_a} \lim_{w'_b \rightarrow w_b} \left[\int_{E_{ab}} \sqrt{T} dw + \frac{\Delta_a}{2} \log(w_a - w'_a) + \frac{\Delta_b}{2} \log(w_b - w'_b) \right] \quad (58)$$

The integration in (58) is performed along edge E_{ab} . The direction of integration is the same as the direction of the edge E_{ab} (see appendix B). Note that the logarithmic terms precisely cancel the divergence from the endpoints of integration in (58) so that the ϖ_{ab} are finite. In going from (56) to (57) we have used the asymptotics for $(s_a \wedge s_b)$ derived in appendix B.

Expanding (57) around $\theta \rightarrow -\infty$, and comparing with (26) with $\xi = e^{\theta + i\phi}$ we read off

$$\int_{E_{ab}} \eta = \int_{\mathbb{R}} \frac{d\theta}{\pi} e^{-\theta - i\phi} \log(1 + A_{ab}^-(\theta + i\phi)) \quad (59)$$

The contour of integration in $\int_{E_{ab}} \eta$ is along the WKB line connecting P_a and P_b and the direction of integration is the same as the direction of the edge E_{ab} . This formula allows us to compute the η -cycles from the χ -functions since the A_{PQ} are explicit functions of the coordinates.

5 The AdS action

5.1 Regularized AdS action

Now that we have introduced the needed tools we are ready to calculate the action (18). We will demonstrate for the case of the 4-point function, but the method is general and could be performed for any number of operators inserted along a line. The computation will be as follows. First we will introduce the relevant WKB triangulation which will be topologically

equivalent to the triangulation shown in figure 9. Second, using the procedure of section 4.8 we will derive the χ -system satisfied by the coordinates of this triangulation. Supplementing these functional relations by the WKB asymptotics we will invert these functional relations using the technique of section 4.9 to obtain a set of integral equations that uniquely determine the coordinates. Finally, from coordinates we extract the η -cycles using the method of section 4.10. Once we have the η -cycles, we compute the action using (18).

5.1.1 Stress-energy tensor and WKB triangulation

For the purpose of the following computation, a useful parameterization of the stress energy tensor is

$$T(w) = \frac{1}{(w - w_4)^2} \left(c_\infty + \frac{c_0 + c_1 w + c_2 w^2 + U w^3}{(1 + w)^2 (1 - w)^2} \right) \quad (60)$$

Here we have fixed three of the insertion points at $w_1 = +1$, $w_2 = \infty$, $w_3 = -1$ using the world-sheet conformal symmetry. The fourth insertion point is left at the position w_4 which should be fixed at the saddle point w_4^* once the full action is assembled. For the purpose of demonstration we will take w_4 to be between $w_3 = -1$ and $w_1 = +1$. When the dominant saddle point is located in one of the other intervals one can proceed by a similar procedure. The constants $c_a = c_a(w_4, \Delta)$ are functions of w_4 and dimensions of the operators and are fixed by the condition (7). Their explicit expressions are given in appendix D. The parameter U is unfixed by the condition (7) and implicitly parameterizes the cross ratio of the four operators (recall that they are inserted along a line in the boundary theory so that there is only one cross ratio). The analytic structure of T , the resulting WKB-structure and the WKB triangulation are shown in figure 15.

5.1.2 χ -system for the 4-point function

From equation (46) and figure 15 we have

$$\chi_{24} \chi_{24}^{++} = \left(\chi_{\hat{2}4} \chi_{\hat{2}4}^{++} \right)^{-1} = \frac{(1 + A_{23})(1 + A_{14})}{(1 + A_{34})(1 + A_{12})} \quad (61)$$

$$\chi_{12} \chi_{12}^{++} = \left(\chi_{14} \chi_{14}^{++} \right)^{-1} = \chi_{34} \chi_{34}^{++} = \left(\chi_{23} \chi_{23}^{++} \right)^{-1} = \frac{(1 + A_{24})}{(1 + A_{24})} \quad (62)$$

To compute each A_{PQ} we use formulas (51) and (49) along with the rules given in figure 14. In that way we find

$$A_{24} = \frac{\chi_{24} (1 + \chi_{12} (1 + \chi_{\hat{2}4} (1 + \chi_{23}))) (1 + \chi_{43} (1 + \chi_{\hat{4}2} (1 + \chi_{41})))}{(1 - \mu_2^2) (1 - \mu_4^2)} \quad (63)$$

$$A_{23} = \frac{\chi_{23} (1 + \chi_{34}) (1 + \chi_{24} (1 + \chi_{12} (1 + \chi_{\hat{2}4})))}{(1 - \mu_2^2) (1 - \mu_3^2)} \quad (64)$$

with the rest of the A_{PQ} being related by relabeling (see appendix D for the explicit formulas). These expressions and equations (61) – (62) provide a closed system of functional equations

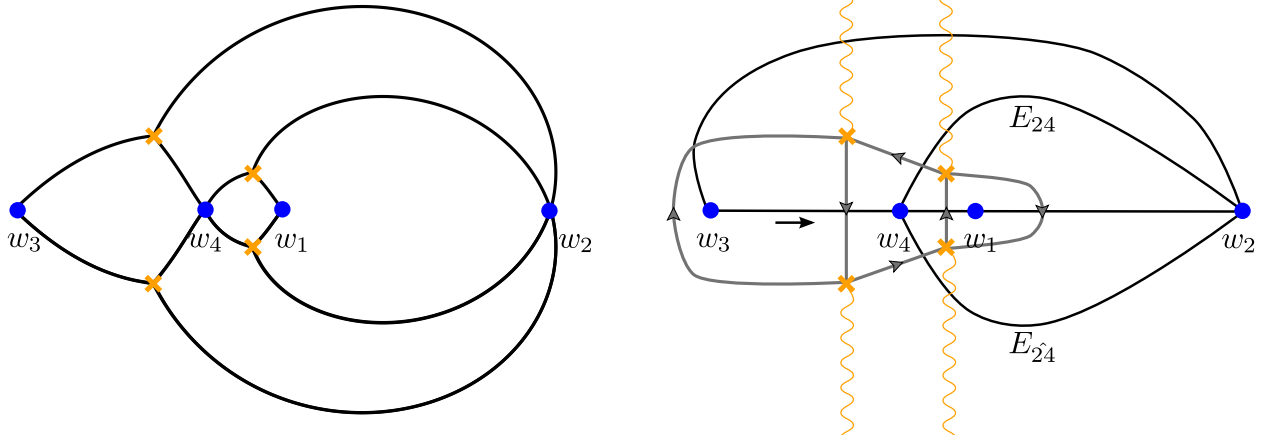


Figure 15: Constructing the triangulation for the 4-point function. In the left panel we show the WKB cells for $\text{Arg}(\xi) = 0$. The cell walls are formed by the separating WKB curves as described in section 4.4; as described there, inside each cell there is a 1-parameter family of generic WKB curves and by taking a representative curve from each family we obtain the triangulation shown in the right panel. In the right panel the black lines are the edges of the WKB triangulation and the wavy yellow lines show our convention for defining the branches of ω . Notice that this triangulation is topologically equivalent to the one shown in figure 9. This means that we can borrow the results derived for that example. In particular, the coordinates can be carried over from that example by making the proper identifications. The cycles corresponding to each coordinate are represented by the gray curves – we show only the portion of each cycle on the sheet of ω where the edge E_{34} has orientation *towards* P_4 as indicated by the black arrow along edge E_{34} .

for the 6 coordinates associated with the triangulation shown in figure 15.

These functional equations can be converted into integral equations of the form (54) using the technique described in section 4.9. To apply the procedure of section 4.9 one must find a ϕ such that the RHS of (52) is decaying, and for this one should appeal to the WKB analysis. The WKB cycles which determine the asymptotics of the coordinates are shown in figure 15. When $\Delta_1 \sim \Delta_3$ and $U \sim 0$, $w_4 \sim 0$ the cycles shown in figure 15 all have $\text{Arg}(\oint_{\gamma_E} \omega) \sim \pi/2$.¹⁶ In this case $\phi = 0$ is a suitable choice since then all χ_E^- will be growing and (53) will decay rapidly.¹⁷ In summary, the integral equations in the region of present interest are given by equations (54) with F_E given by (61) – (64). These equations will remain valid for all values of the parameters Δ_a , U , and w_4 such that the triangulation is unchanged. If one deforms these parameters too much the triangulation will jump. One can then easily write the χ -system for the new triangulation and apply the same procedure to obtain the integral

¹⁶Interestingly, when $\Delta_1 = \Delta_3$ and $U = w_4 = 0$ there is a symmetry which causes the RHS of the χ -system to trivialize (i.e. to reduce to 1 for all χ_E) and the χ -functions can be computed explicitly (they are just equal to their zero-mode part). This is reminiscent of the case for the three-point function and, in fact, there is also a change of coordinates that maps the specific case $\Delta_1 = \Delta_3$ and $U = w_4 = 0$ to two copies of a three-point function.

¹⁷This will continue to be the case as long as the $\text{Arg}(\oint_{\gamma_E} \omega)$ remain in the upper-half plane. In other-words, the inversion procedure will be valid for all U and w_4 such that the triangulation is unchanged since the triangulation will jump precisely when one of the $\oint_{\gamma_E} \omega$ crosses the real-axis [12].

equations for that region of parameters.¹⁸

By numerically iterating these equations (using $\chi_E^{(0)}$ as the initial iterate for each χ_E) we obtain the χ -functions. The η -cycles are then extracted from the χ -functions using the procedure of section (4.10). In the following section we will write the regularized *AdS* action in terms of these η -cycles.

5.1.3 Finite part of *AdS* action

Now that we are able to compute the η -cycles (see previous subsection) we can use the formula

$$A_{fin} = \int_{\Sigma} \sqrt{T\bar{T}} (\cosh \gamma - 1) = \frac{\pi}{3} - \frac{i}{2} \left(\oint_{\gamma_a} \omega \right) I_{ab}^{-1} \left(\oint_{\gamma_b} \eta \right). \quad (65)$$

(see section 3.2 and equation (18)) to compute the regularized part of the *AdS* action. To use (65) there are few steps. These steps are simple but tedious and we will only list them here (see appendix D for a detailed implementation). As described in section 3.2 one should first modify T by spreading the double poles slightly such that $\omega = \sqrt{T}dw$ has an additional square-root cut at each of these points. Then one should choose a complete basis of a - and b -cycles (five of each is needed for the 4-point function). One can then apply formula (18) and then take the limit in which the small cuts close to form simple poles in ω . Once this is done the area will generically be expressed in terms of three different types of η -cycles: cycles connecting two punctures, cycles connecting a puncture with a zero and cycles connecting two zeros. The latter two can be expressed as linear combinations of the puncture-puncture cycles as described in appendix D. Once this is done, the final result takes the elegant form

$$A_{fin} = \frac{\pi}{3} - i \sum_{E \in \mathcal{T}} \omega_E \eta_E \quad (66)$$

where the sum runs over the edges in the triangulation (see figure 15), $\eta_{E_{ab}}$ is defined in (59) while $\omega_{E_{ab}}$ is the ω -cycles that intersects edge E_{ab} (i.e. the integral of ω that is associated with the coordinate χ_{ab} ; these integrals are shown as the gray contours in figure 15).¹⁹

Formula (66) and the procedure of section 4 for computing the η -cycles solve the problem of computing the regularized *AdS* contribution to the 4-point function. In the next section we present some numerical tests of the procedure. Let us note that the procedure of section 4 is general and can be implemented for any number of punctures. Further, while we have only proved equation (66) for the case of the 4-point function, given its simplicity one might suspect that the formula holds in general (with $\pi/3 \rightarrow \pi/12 \times (\#\text{number of zeros of } T)$, of course).²⁰ Even if the general result does not take the simple form (66), for a given T (i.e. for any number of punctures) the procedure described in section 3.2 is still valid and one can still write A_{fin} in terms of the η_E for the corresponding triangulation). In principle this

¹⁸Another (more elegant) approach would be to find a systematic way of analytically continuing the integral equations from one region of parameters to another as was done for the TBA equations of [10].

¹⁹Note that in formula (66) both integrals ω_E and η_E are the *segment* integrals between the appropriate limits. For example, the $\omega_E = \frac{1}{2} \oint_{\gamma_E} \omega$. In this sense we are abusive with the term ‘cycle’.

²⁰It would be a simple matter to check this, but we have not pursued this issue. We did check that the formula holds for the 3-point function (see appendix E).

U	Δ_3	Δ_4	Δ_1	Δ_2	Numerics	χ -system
1/5	1	2	1	2	0.84807	0.84812
1/2	1	2	1	2	0.82421	0.82423

Table 1: Comparison of the A_{fin} obtained by numerically integrating (10) and the area computed from the χ -system. The results are for the spike configuration of figure 4B.

solves the problem of computing the regularized AdS contribution to the N -point function. We have performed numerical tests only for the case of the 4-point function. We present these numerical results in the following section.

5.1.4 Numerical tests

We now present numerical tests of the method described above. We solved numerically the modified sinh-Gordon equation (10) for the function γ and then using this numerical solution to directly compute A_{fin} via

$$\int_{\Sigma} \sqrt{T\bar{T}} (\cosh \gamma - 1) \quad (67)$$

The general set-up of the numerical problem essentially follows that of [8] with some modifications. However, the numerical method that we use to solve the PDE (10) is quite different from that of [8].²¹ We place the punctures at $w_3 = -1$, $w_4 = 0$, $w_1 = 1$, and $w_2 = \infty$. We then map the sphere to a square domain with the point at infinity mapping to the boundary of the square and the real axis mapping onto itself. Since γ must vanish at the punctures, we should impose $\gamma = 0$ along the boundary of the square domain since w_2 maps to the boundary of the square in the new coordinates. Further, since for either configuration of spikes (see section 3.3 and figure 4) there is a fold-line along the real axis, we know $\gamma(x, 0) = 0$ where we are using the coordinates $w = x + iy$ and writing $\gamma = \gamma(x, y)$. Thus we can solve the problem in half of the square with the Dirichlet boundary conditions $\gamma = 0$ on the boundaries. Lastly, we must remove the logarithmic singularities (11) in order to have a nice smooth function to solve for. A suitable function is

$$2\gamma_{reg} = \gamma + \frac{1}{2} \sum_a \sigma_a \log \left[\frac{(w - z_a)(\bar{w} - z_a)}{(1 + w\bar{w})} \right] \quad (68)$$

where we $\sigma_a = \pm 1$ is determined by $\gamma \sim -\sigma_a \frac{1}{2} \log T\bar{T}$ at z_a . The numerator of (68) removes the log divergences (11) in γ while the denominator is included to kill off these additional log terms at infinity. In the numerical implementation we fix the spike configuration we want to describe by choosing the set of $\{\sigma_a\}$. Finally, to numerically integrate the equation (10) (re-written in terms of γ_{reg} , of course) we use a standard relaxation method with an uniform grid.

In table 1 we compare the numerical results with the analytic results. The numerical

²¹We are very grateful to Romuald Janik for providing us with a copy of the code used in [8] which was very useful in helping us to develop and test our own numerics.

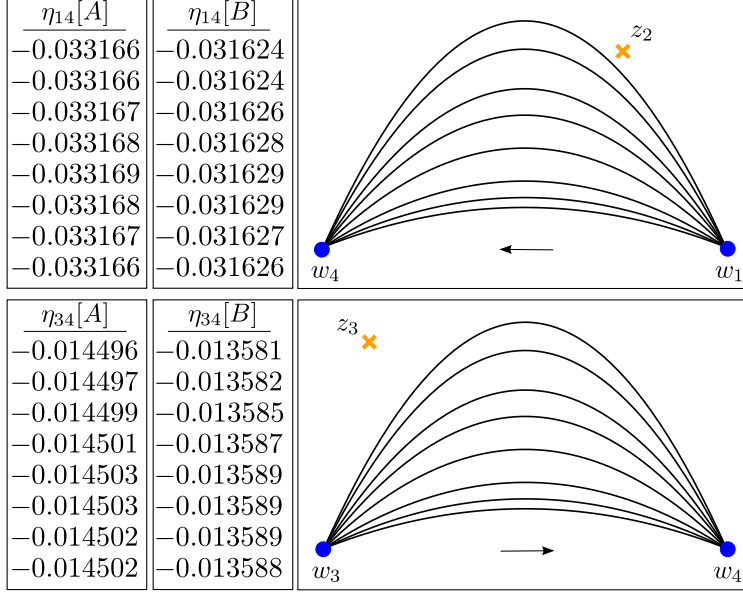


Figure 16: Here we show the values of η_{14} and η_{34} evaluated along several different contours. For example, the column labeled $\eta_{14}[A]([B])$ shows the values of η_{14} for the spike configuration of figure 4A(B) for each of the contours shown to the right of the column. We use the parameter values $\Delta_3 = \Delta_1 = 1$, $\Delta_2 = \Delta_4 = 2$ and $U = 1/5$ for both spike configurations. There are five digits that we trust since they are unchanged for the different contours and they should be compared with our result from the functional equations that is $\eta_{14}^{\chi\text{-system}}[A] \approx -0.033169$, $\eta_{34}^{\chi\text{-system}}[A] \approx -0.014503$ and $\eta_{14}^{\chi\text{-system}}[B] \approx -0.031628$, $\eta_{34}^{\chi\text{-system}}[B] \approx -0.013588$. In the digits where the forms are closed there is perfect agreement with the analytic results.

results are obtained by the area computed using (67) with the numerical solution for γ . The analytic result is obtained from (66) with the η -cycles computed using the χ -system procedure. These results show a good agreement of our formula with the numerics.

A sharper measure of the agreement between the analytics and numerics is to compare directly the η -cycles. In figure 16 we show the numerical results for η_{14} and η_{34} computed along several different contours. This allows us to test the closure of the numerical η which we obtain from the numerical γ via (16). Note that closure of η implies that γ must obey (10) and thus this is a good measure of the numerical error. Indeed, one can see in figure 16 that the numerical cycles agree with the analytical predictions in all digits in which they are closed. That is, the numerics is in agreement with the analytics in all of the digits for which the numerics can be trusted.

Finally, it would be interesting to perform numerical tests for a larger portion of the parameter space (i.e. more values of the Δ_a , U and w_4). To perform a systematic study will probably require an improvement of our numerical method as our current method, while extremely simple, has very slow convergence.

5.2 Divergent part

In section 5.1 we completed the task of computing the first term in formula (14). In this section we will discuss the second term

$$- \int_{\Sigma \setminus \{\epsilon_a\}} d^2w \sqrt{T\bar{T}} = -\frac{\pi}{2} \sum_a \Delta_a^2 \log \epsilon_a - A_{reg} \quad (69)$$

where A_{reg} is finite at $\epsilon_a \rightarrow 0$. The contribution A_{reg} can be computed by simple but tedious application of the Riemann bilinear identity and there are many ways to write the result. For example

$$A_{reg} = i \sum_{E \in \mathcal{T}} \varpi_E \omega_E - i \frac{1}{2} (\varpi_{24} - \varpi_{\bar{2}4}) (\omega_{24} - \omega_{\bar{2}4}) \quad (70)$$

where the sum is over the triangulation shown in figure 15 and $\varpi_{E_{ab}} \equiv \varpi_{ab}$ is defined in (58). The ω_E are defined in the same way as in (66). One can check this formula by comparing with the direct 2D numerical integration of $\sqrt{T\bar{T}}$ with small circular disks cut out around the puncture (in Mathematica one can use `NIntegrate` along with the `Boole` command, for example).

We recall that (69) came from the regularization of the string action where we have added and subtracted $\sqrt{T\bar{T}}$ from the integrand of the *AdS* action. This integral depends explicitly on the cut-off ϵ_a around the punctures. It will be important to understand the connection with the physical cut-off \mathcal{E} at the boundary of *AdS*. Fortunately we can extract the needed information from the linear problem since we have good analytic control over the solutions near the insertion points. To proceed by this route (which parallels the discussion of [8] for the 3-point function) we must first describe how the string embedding coordinates are recovered from the linear problem formalism, which is via the aptly-named *reconstruction formulas*. We will discuss this in the next subsection, 5.2.1. After that, in section 5.2.2 we will use the reconstruction formulas to eliminate the ϵ_a in favor of \mathcal{E} . From this procedure we will recover the standard spacetime dependence in (1) along with a contribution to the function $f(u, v)$. This will complete the computation of the semiclassical *AdS* contribution to (1).

5.2.1 Reconstruction formulas

The reconstruction formulas allow us to express the string embedding coordinates in terms of solutions of the linear problem. This point is crucial in our construction for the following reasons. First, we have introduced some regulators in the world-sheet, ϵ_a , that must be related to the physical cut-off in the boundary of *AdS*, $z = \mathcal{E}$. Second, by using them we will be able make the spatial dependence explicit in the final result, namely the insertion points x_a of the operators in the gauge theory.

Consider two solutions of the linear problem, ψ_A and ψ_B normalized as $(\psi_A \wedge \psi_B) = 1$, and construct a matrix Ψ as

$$\Psi = (\psi_A \ \psi_B). \quad (71)$$

The matrix Ψ obeys the same equations of motion as $\psi_{A,B}$ (19), namely

$$(\partial + J_w)\Psi = 0, \quad (\bar{\partial} + J_{\bar{w}})\Psi = 0. \quad (72)$$

where J_w and $J_{\bar{w}}$ are defined in (19)-(20). One can verify using (9) that the quantity

$$y^I \equiv -\frac{1}{2} \text{tr} \left(\tilde{\sigma}^I \sigma^2 \Psi^T \sigma^1 \Psi \right) \Big|_{\theta=0} \quad (73)$$

with $\tilde{\sigma}^1 = \sigma^1$, $\tilde{\sigma}^2 = -i\sigma^2$, $\tilde{\sigma}^3 = \sigma^3$, satisfies the same equations of motion as Y^I and also the constraint $y \cdot y = -1$ (with the *AdS* metric). In this way we establish a correspondence between target space coordinates and solutions of the linear problem,

$$\frac{1}{z} = Y^2 - Y^1 = 2i \Psi_{11} \Psi_{21}, \quad \frac{x}{z} = Y^3 = i(\Psi_{11} \Psi_{22} + \Psi_{12} \Psi_{21}) \quad (74)$$

In order to relate the operator insertion points x_a and physical cut-off \mathcal{E} with the linear problem data, it is convenient to express ψ_A and ψ_B in terms of the elementary solutions s_a and \tilde{s}_a whose behavior close to the punctures is given by (21),

$$\psi_A = (\psi_A \wedge \tilde{s}_a) s_a + (s_a \wedge \psi_A) \tilde{s}_a, \quad \psi_B = (\psi_B \wedge \tilde{s}_a) s_a + (s_a \wedge \psi_B) \tilde{s}_a \quad (75)$$

Close to the punctures the solution \tilde{s}_a becomes dominant. Then, using (74) and the explicit form of \tilde{s}_a close to the puncture P_a we get that

$$z = \frac{1}{i(s_a \wedge \psi_A)_0^2} |w - w_a|^{\Delta_a} \quad (76)$$

where the subscript 0 indicates that the solutions are evaluated at $\theta = 0$ (recall that this is the value where the physical problem is recovered – see equation (73)). Equation (76) is the relation needed to make the connection between the world-sheet and physical cut-off's

$$\Delta_a \log \epsilon_a = \log \mathcal{E} + \log |(s_a \wedge \psi_A)|_0^2 \quad (77)$$

Finally, using once again (74) we express the insertion points x_a of the operators in the gauge theory as

$$x_a = \frac{(s_a \wedge \psi_B)_0}{(s_a \wedge \psi_A)_0} \quad (78)$$

5.2.2 Physical regulator and spacetime dependence

We can now use (77) to eliminate the ϵ_a in (69) in favor of the physical cut-off at the boundary of AdS $z = \mathcal{E}$. We have

$$\sum_a \Delta_a^2 \log \epsilon_a = \left(\sum_a \Delta_a \log \mathcal{E} + \sum_a \Delta_a \log |(s_a \wedge \psi_A)|_0^2 \right) \quad (79)$$

where a and A refer respectively to the small solution s_a and one generic solution ψ_A appearing in the reconstruction formulas. Now we will eliminate the factors $|(s_a \wedge \psi_A)|_0$ in terms

of objects that we can compute.

The terms $|(s_a \wedge \psi_A)|_0^2$ can be related to the insertion points x_a in target space and overlaps of the elementary solutions evaluated at $\theta = 0$ through expression (78). Using Schouten's identity one can verify that

$$|(s_a \wedge \psi_A)|_0^2 = \frac{x_{bc}}{x_{ba}x_{ca}} \frac{|(s_b \wedge s_a)|_0 |(s_c \wedge s_a)|_0}{|(s_c \wedge s_b)|_0} \quad (80)$$

for a, b, c distinct. This solution is unique up to different ways of rewriting the spatial dependence using the cross-ratio

$$u = \frac{x_{14}x_{23}}{x_{12}x_{34}} = \frac{(s_1 \wedge s_4)_0 (s_2 \wedge s_3)_0}{(s_1 \wedge s_2)_0 (s_3 \wedge s_4)_0} \quad (81)$$

where we have used (78). Note that we can compute the brackets appearing in (77)-(78) using (57). In particular we have

$$\log (s_a \wedge s_b)_0 = \left(\frac{1}{2} \varpi_{ab} + \frac{1}{2} \bar{\varpi}_{ab} \right) + \int_{\mathbb{R}} \frac{d\theta \log(1 + A_{ab}^-)}{2\pi \cosh \theta} \quad (82)$$

This formula is valid when there is a WKB line connecting P_a and P_b . If a bracket appears for which we do not have a WKB line, we can simply use the cross ratio (81) to eliminate it in terms of brackets that can be computed using (82).

Finally, using (80) in (79) and massaging the resulting spacetime dependence by extracting multiples of u and $(1 + u)$ we find

$$e^{2 \times \frac{\sqrt{\lambda}}{2} \Delta_a^2 \log \epsilon_a} = \prod_{a>b}^4 (|s_a \wedge s_b|_0)^{-\sqrt{\lambda} \Delta_{ab}} \left(\frac{x_{ab}}{\mathcal{E}} \right)^{\sqrt{\lambda} \Delta_{ab}} \quad (83)$$

where $\Delta_{ab} = (\sum_c \Delta_c) / 3 - \Delta_a - \Delta_b$. The extra factor of 2 in the exponent on the left hand side of (83) anticipates the sphere regularization which turns out to be similar to the AdS part and will be treated in section 6.1.

We recognize in (83) the canonical spacetime dependence in the 4-point function of a conformal field theory (compare with equation (1)). The appearance of the cut-off in (83) is related to the renormalization of the operators. In fact, if we define $\tilde{\mathcal{O}}_{\Delta_a} \equiv \mathcal{E}^{\Delta_a} \mathcal{O}_{\Delta_a}$ this will cancel the \mathcal{E} factors in (83). To be more precise, we should define a 4-point function that is independent of the operator renormalization. The standard procedure is to divide by the appropriate product of 2-point functions such that normalization factors cancel. The same factors of \mathcal{E} will appear in these 2-point functions and will cancel with those in (83). We will thus drop the factors of \mathcal{E} in the formulas below.

5.3 Summary of the AdS and divergent contributions

We have now computed all the parts of (14). In this section we summarize the full result. The semiclassical limit of the 4-point function (1) is given by

$$\left(\int_{fin}^{AdS} \int_{div}^{AdS \times S} \int_{fin}^S \right)^* \prod_{a<b}^4 (x_{ab})^{\Delta_{ab}}, \quad (84)$$

where the $*$ denotes evaluation at $w_4 = w_4^*$ and we define

$$f_{fin}^{AdS}(w_4) = e^{-\frac{\sqrt{\lambda}}{\pi} A_{fin}} \quad (85)$$

$$f_{div}^{AdS \times S}(w_4) = e^{-2\frac{\sqrt{\lambda}}{\pi} A_{reg}} \prod_{a>b}^4 (|s_a \wedge s_b|_0)^{-\sqrt{\lambda} \Delta_{ab}} \quad (86)$$

and f_{fin}^S will be defined momentarily. The contribution A_{fin} is given by (66), A_{reg} is given in (70), the brackets in $f_{div}^{AdS \times S}$ are given by (82).

The sphere part of the correlation function contains divergences of the same type as AdS . We therefore regularize it also by subtracting $\sqrt{T\bar{T}}$. Such finite contribution is what we denote by f_{fin}^S

$$f_{fin}^S \equiv e^{-\frac{\sqrt{\lambda}}{\pi} \int_{\Sigma} (S^5 \text{ contribution} - \sqrt{T\bar{T}})} \quad (87)$$

where S^5 contribution stands for the S^5 Lagrangian and wavefunctions [8]. To compensate this subtraction, we include the factor of 2 in front of A_{reg} in expression (86). In general we cannot complete the construction of the 4-point function because we are unable to compute the contribution f_{fin}^S . Fortunately, for correlators involving only BPS operators of the same type (e.g. only Z and \bar{Z}) the sphere part is known and we can assemble the full result. This is the subject of the next section.

6 Full correlation function for BMN operators

In this section we compute the full correlation function for operators of the type $\text{tr } Z^{\Delta}$ when Δ scales as $\sqrt{\lambda}$. For these type of operators, the sphere part f_{fin}^S was already known [31] and therefore we can complete our computation. We stress that, unlike the three point function, this four point correlator is not protected. In section 6.2, we fix the location of the puncture w_4 by the saddle point method and discuss some issues on the multiple string embedding configurations. In section 6.4 we perform an analytical check of our procedure by studying the extremal limit where $\Delta_2 = \Delta_1 + \Delta_3 + \Delta_4$, which is known to be protected from quantum corrections.

6.1 Sphere part

The sphere part of the correlation function involves the classical wave-functions associated to the external states. We consider specifically the correlation function of four BMN operators²²

$$\langle \text{tr } Z^{\hat{\Delta}_1}(x_1) \text{tr } Z^{\hat{\Delta}_2}(x_2) \text{tr } \bar{Z}^{\hat{\Delta}_3}(x_3) \text{tr } \bar{Z}^{\hat{\Delta}_4}(x_4) \rangle, \quad (88)$$

for which the wave-functions are known [13, 14]. The string dual of these operators corresponds geometrically to a string that is point-like in the sphere and rotates around an equator [15]. The surface developed by the worldsheet is not extended in the sphere.

²²We are using the following notation for the dimensions of the operators $\hat{\Delta}_a = \sqrt{\lambda} \Delta_a$.

Let X_i ($i = 1, \dots, 6$) be the coordinates in S^5 . This particular string state can be expressed as

$$X_1 + iX_2 = e^{i\varphi} \quad X_i = 0, \quad i = 3, \dots, 6 \quad (89)$$

where φ is an azimuthal angle of the sphere. The wave-functions for $\text{tr } Z^{\hat{\Delta}_a}$ and $\text{tr } \bar{Z}^{\hat{\Delta}_a}$ are given respectively by

$$\Psi_{\hat{\Delta}_a} = e^{i\hat{\Delta}_a\varphi(w_a, \bar{w}_a)}, \quad \bar{\Psi}_{\hat{\Delta}_a} = e^{-i\hat{\Delta}_a\varphi(w_a, \bar{w}_a)} \quad (90)$$

where the field φ is evaluated at the puncture corresponding to the respective operator insertion.

As the wave-functions scale exponentially with $\sqrt{\lambda}$, they will act as sources for the equations of motion for φ . The total sphere contribution is then given by

$$\exp \left[-\frac{\sqrt{\lambda}}{\pi} \left(\int d^2w \partial\varphi\bar{\partial}\varphi + i\pi (\Delta_3\varphi_{w=-1} + \Delta_4\varphi_{w=w_4} - \Delta_1\varphi_{w=1} - \Delta_2\varphi_{w=\infty}) \right) \right]. \quad (91)$$

Considering both the contributions from the S^5 action and wave-functions as an effective action, we obtain the equations of motion for φ which are solved by

$$\varphi(w, \bar{w}) = i (\Delta_3 \log |w + 1| + \Delta_4 \log |w - w_4| - \Delta_1 \log |w - 1|). \quad (92)$$

This solution has an additional singularity at infinity with charge $-\Delta_3 - \Delta_4 + \Delta_1 (\equiv -\Delta_2)$, corresponding to the wave-function inserted at infinity. This is consistent with R -charge conservation. We may now plug (92) into (91), introducing cut-off's around the punctures to regulate this contribution. This amounts to evaluate the solution at a distance ϵ away from the punctures. As in the case of the AdS action, the logarithmic divergences

$$\exp \left[\frac{\sqrt{\lambda}}{2} \sum_i \Delta_i^2 \log \epsilon_i \right] \quad (93)$$

need to be regularized. We do this by subtracting $\sqrt{T\bar{T}}$ from the integrand. To compensate, we add a similar contribution to the divergent part, that was already treated in the previous section (indeed, this regularization procedure is responsible for the factor of 2 appearing in front of A_{reg} in expression for $f_{div}^{AdS \times S}$, see (86)). The dependence on the cut-off's then disappears yielding the following expression for the regularized sphere action and wave-functions

$$f_{fin}^S = \exp \left[\sqrt{\lambda} \left(A_{reg} - \log 2^{\Delta_3\Delta_1} - \log \frac{|w_4 - 1|^{\Delta_1\Delta_4}}{|w_4 + 1|^{\Delta_3\Delta_4}} \right) \right], \quad (94)$$

where f_{fin}^S was defined in (87)

6.2 Saddle point determination

We have shown how to compute the quantities (85)-(86) as a general function of w_4 . However, to compute (84) we must evaluate at the saddle point $w_4 = w_4^*$. Before discussing how to

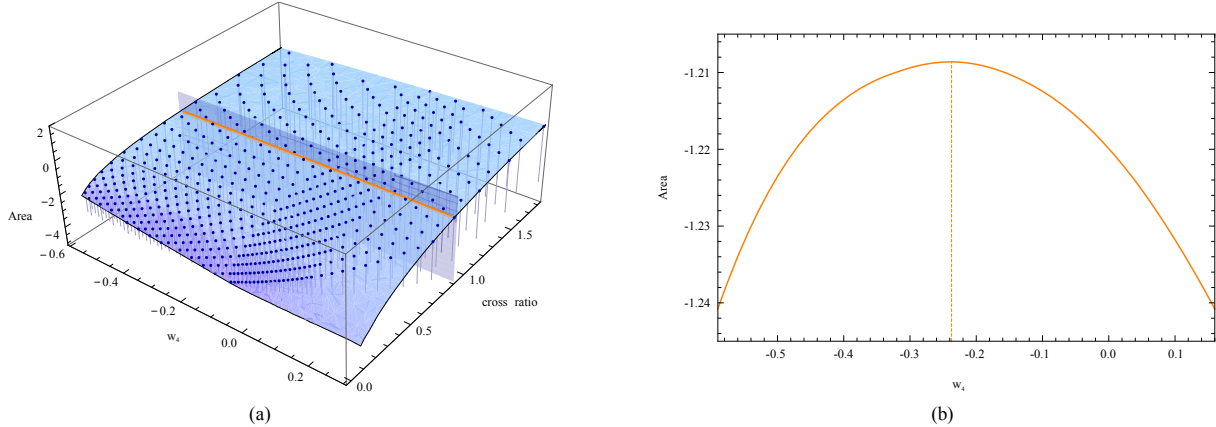


Figure 17: In (a) we computed several points for a region around $u \sim 0.9$ and interpolated the surface in blue. We then took a constant cross ratio slice. The intersection is given by the orange line. In (b) we have plotted the area as function of w_4 for cross ratio $u = 0.9$, where we have a saddle point at $w_4^* \approx -0.24$.

locate the saddle point for generic values of the parameters, let us discuss a very symmetrical situation in which we can guess its position.

Using conformal symmetry, we can fix three of the points in the target space at $x_3 = -1, x_1 = 1$ and $x_2 = \infty$ and also in the world-sheet at $w_3 = -1, w_1 = 1$ and $w_2 = \infty$. The fourth point x_4 will then be related to the cross ratio. For the particular choice of the cross ratio (81) equal to 1, the fourth point will be located at zero. Moreover if we choose the points at $x_3 = -1$ and $x_1 = +1$ to have the same conformal dimension and the same type of fields (say Z 's) then this is a very symmetrical configuration. Going back to the world-sheet coordinates, by symmetry we expect to find the saddle point at $w_4^* = 0$.

Let us now describe how we determine the saddle point in practice. All the physical information that we input is contained on the stress-energy tensor. Besides the conformal dimensions of the operators and the position of the punctures, there is the extra parameter U that translates the additional degree of freedom of the cross ratio. The two are implicitly connected by the expression

$$\chi_{24}(\theta = 0; U) = \frac{x_{14} x_{23}}{x_{12} x_{34}} \equiv u \quad (95)$$

by formulas (81) and (34). Therefore, our strategy will be to compute the area and cross ratio for many points in a region in the (w_4, U) plane and then translate that information to the (w_4, u) plane. Finally, we take slices of constant cross ratio, and determine for which w_4 the area is stationary.²³ We can very easily perturb away from this very symmetrical configuration and track the location of the saddle point. For example, in figure 6.2, we have found a saddle point for $u = 0.9$ at $w_4^* \approx -0.24$. One can compute the location of w_4^* to arbitrary numerical accuracy by iterating the χ -system; here we present only 2 digits since we just want to demonstrate the procedure for locating the saddle point. In the following

²³In this way one can confirm that indeed $w_4^* = 0$ for the very symmetrical configuration described above.

section we will discuss the issue of the multiple saddle points and connect with the discussion of section 3.3 about the different configurations for the string embeddings in AdS_2 .

6.3 Saddle points and multiple string configurations

In section 2 and appendix C, we discussed the different AdS_2 string embedding geometries and its connection with the different boundary conditions (11) that one can impose on γ . At the level of the functional equations, we have seen that the different boundary conditions manifest in the different $\xi \rightarrow 0, \infty$ asymptotics of the coordinates. More precisely they will affect the constant $C_E^{(0)}$ in the expression (40). One may ask which of the configurations in figure 2 we should find given a cross ratio and a set of conformal dimensions. We have already introduced this question but let us make it more precise now that we have all the tools in hand.

Consider the example of the WKB triangulation we have been studying. There exist *a priori* two choices for the orientations of the spikes, as discussed in section 3.3 and appendix C. Consider the spike configuration of figure 4A, which is the one used for the saddle-point analysis of section 6.2. Recall that for this case the cross ratio $u = \chi_{24}(\theta = 0) \approx 0.9$ is *positive*. This means that the point x_4 is located between x_3 and x_1 . Furthermore, we have found a saddle point located in $-1 < w_4^* < +1$. Looking at figure 1 we see that this situation corresponds to a case in which the insertions do not cross since $x_3 < x_4 < x_2$ and $w_3 < w_4^* < w_1$.²⁴ Since the insertions do not cross, we expect the string embedding to be that of figure 2A.

Now, one might expect that the configuration in figure 2B can be described simply by considering the spike configuration of figure 4B *but keeping the same saddle point* $w_3 < w_4^* < w_1$ and the same value of the cross ratio as in the previous spike configuration. However, this is not possible since in this new spike configuration the cycle for χ_{24} connects two spikes of the same type and thus from (40) we see that it will acquire an overall factor of (-1) so that $u < 0$.²⁵

The point is that if we *fix* a cross ratio u and then consider a specific saddle-point w_4^* then the orientation of the spikes *is fixed* and thus the configuration of the string embedding is also fixed. This is in perfect agreement with the mapping between figure 1 and 2 and it is non-trivial that the integral equations encode this mapping.

Given the above discussion, we are confronted with a very interesting possibility. Generically we do not expect the saddle point w_4^* to be unique and it's likely that there are actually several saddle points $w_{4^*}^{(i)}$ on the 4-punctured sphere. As per the above discussion, for fixed u , Δ_a and a given $w_{4^*}^{(i)}$ the corresponding string embedding is fixed.²⁶ In particular, if there is a saddle point in each of the three intervals of the real axis we should examine each of

²⁴Be aware that the ordering of the x_a in this discussion is different from that used in figure 1.

²⁵Of course the corrections to χ_{24} from iterating the integral equations will differ for the two different spike configurations but they should not change the overall sign of $\chi_{24}^{(0)}$. We are taking this as a physically motivated assumption in this discussion. We have checked this assumption in a few examples and found that it holds.

²⁶Note that for fixed u , Δ_a the triangulation will depend on which $w_{4^*}^{(i)}$ one is considering. This is not a problem as one can apply the method of section 4 to each of these triangulations individually.

these in turn.²⁷ For a fixed u , two of these will be double-folded and one will be single-folded. One should find all of these saddle points and determine which is the dominant one, which is equivalent to ask which string embedding configuration is dominant. One may even find a dependence of the dominant string configuration on the dimensions of the operators thus giving rise to phase transitions between configurations. The issue of finding the different saddle points and their dependence on the parameters of the theory certainly deserves a deeper study.

6.4 Extremal Limit

In this section, we study the correlation function

$$\langle \text{tr } \bar{Z}^{\hat{\Delta}}(x_1) \text{tr } Z^{\hat{\Delta}_2}(x_2) \text{tr } \bar{Z}^{\hat{\Delta}}(x_3) \text{tr } \bar{Z}^{\hat{\Delta}_4}(x_4) \rangle \quad (96)$$

in the extremal limit when

$$\Delta_2 = 2\Delta + \Delta_4. \quad (97)$$

Such correlator is protected from quantum corrections as conjectured in [16] and later proved in [17]. Thus, we expect to obtain the tree level gauge theory result which in the planar limit is simply given by Wick contractions

$$\frac{1}{x_{12}^{2\hat{\Delta}} x_{23}^{2\hat{\Delta}} x_{24}^{2\hat{\Delta}_4}}. \quad (98)$$

The AdS part of our formula is universal in the sense that it only depends on the dimensions of the operators. On the other hand, the sphere part of the correlation function involves the precise details of the operators inserted. Compared to the previous sphere calculation (88), computing (96) just amounts to take the complex conjugate of the wave function located at x_1 , due to the replacement of $Z \rightarrow \bar{Z}$.

Let us start by studying the case when the cross ratio is $u = 1$, where we know the saddle point is $w_4^* = 0$. From this we will be able to see the general mechanism that gives the expected simplification of our result. The first important observation is that in this limit the zeros of $T(w)$ collide on the real axis as depicted in figure 18. Let us start by analyzing what this implies at the level of the χ -system. As the integrals ω_{14} and ω_{34} vanish, the χ 's associated to these cycles, namely χ_{34} and χ_{14} , tend to -1 . This observation has the remarkable consequence that the right hand side of all equations in the χ -system becomes trivially equal to 1 as one can easily verify²⁸. As a result, all χ -functions are *exactly* given by

²⁷Here we are not considering the possibility of complex-conjugate pairs of saddle points located off of the real axis (see footnote 2).

²⁸This trivialization of the χ -system is general and follows *just* from the fact that the two cycles ω_{14} and ω_{34} vanish which implies that the χ -functions χ_{34} and χ_{14} become -1. In the specific case of $U = w_4 = 0$ and $\Delta_1 = \Delta_3$, which turns out to correspond to cross ratio 1, the χ -system is already trivial because of the symmetry of the stress energy tensor in this particular point of the parameter space, see footnote 16). Nevertheless, we emphasize that the trivialization of the χ -system in general does not rely on this specific symmetry of the stress energy tensor.

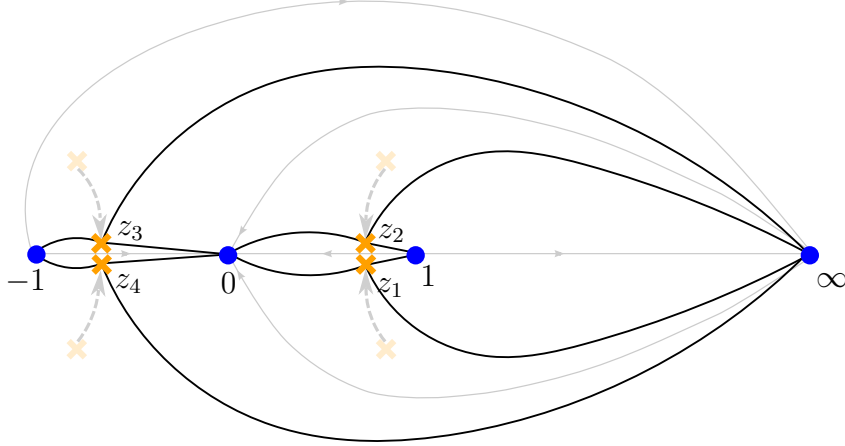


Figure 18: In the extremal limit, the main feature is that the zeros collide on the real axis. The black lines represent the WKB cells whereas the gray lines represent the WKB triangulation. At the exact extremal configuration, there are no WKB lines connecting 1 to 0 nor -1 to 0. We interpret this as a manifestation of the field theory fact that at tree level all operators are Wick contracted only to the fourth operator.

leading term of the WKB expansion (40)²⁹. For convenience, let us introduce an infinitesimal δ defined by the condition $\delta = 2\Delta + \Delta_4 - \Delta_2$. At the end of the day, we will take $\delta \rightarrow 0$. In this limit, the solutions of the χ -system are then given by

$$\chi_{23} = \chi_{12} = -e^{-\frac{\pi(4\Delta-\delta)}{2} \cosh \theta}, \quad \chi_{34} = \chi_{14} = -e^{-\frac{\pi\delta}{2} \cosh \theta}, \quad \chi_{24} = \chi_{24} = e^{-\frac{\pi(2\Delta_z-\delta)}{2} \cosh \theta} \quad (99)$$

We may now plug this solution in the expression (51) and extract the cycles using as described in section 4.10. We find that all A 's vanish in the limit $\delta \rightarrow 0$ except for A_{14} and A_{34} , which tend to -1 as δ goes to zero. This implies that all $\eta_{E_{ab}}$ vanish except for η_{14} and η_{34} , which diverge since the integrand of these cycles becomes singular in this limit. However, one must go back to the area formula (66) and realize that such cycles are multiplied by a vanishing quantity. Indeed, (66) simplifies to

$$\frac{1}{4}\pi\delta\eta_{14} + \frac{\pi}{3}. \quad (100)$$

In the limit $\delta \rightarrow 0$, the first term of this expression is explicitly given by

$$\delta \int_0^\infty d\theta \cosh \theta \log \left(1 - e^{-\frac{1}{2}\pi\delta \cosh \theta} \right) + \mathcal{O}(\delta) = -\frac{\pi}{3} + \mathcal{O}(\delta). \quad (101)$$

Hence, it turns out that the finite AdS contribution vanishes in the extremal limit. We believe this is the general mechanism for any value of the cross ratio.

The computation of the sphere contribution follows the same steps as before, with a slight change on one vertex operator (recall that to get the extremal case, we replaced the operator located at x_1 in (88) by $\text{tr } \bar{Z}^{\hat{\Delta}}$). The new solution for the equations of motion is

$$\varphi(w, \bar{w}) = i \left(\Delta \log |w + 1| + \Delta_4 \log |w| + \Delta \log |w - 1| \right). \quad (102)$$

²⁹Indeed, when the right hand side of the χ -system is 1, the kernel term in equation (54) vanishes and we are left with leading WKB contribution.

Now when we compute the contribution of the sphere action and wavefunctions on this solution, we find that it *exactly* cancels the term \sqrt{TT} for Δ 's satisfying (97). Consequently, the sphere part of the correlation function also vanishes in the extremal limit.

The divergent piece in the extremal becomes simply

$$e^{-\frac{\sqrt{\lambda}}{\pi} A_{reg}} \prod_{a>b}^4 (|s_a \wedge s_b|_0)^{-\sqrt{\lambda} \Delta_{ab}} \rightarrow \delta \int_{-\infty}^{\infty} \frac{d\theta}{2\pi \cosh \theta} \log(1 - e^{-\frac{1}{2}\pi\delta \cosh \theta}) + \mathcal{O}(\delta) = \frac{\delta}{\pi} \log \frac{\pi\delta}{2} + \mathcal{O}(\delta) \quad (103)$$

which goes to zero as $\delta \rightarrow 0$. We are left with the spatial dependent part which, using that the cross-ratio is 1, can be written as

$$\frac{1}{\left(\frac{x_{12}}{\varepsilon}\right)^{2\hat{\Delta}} \left(\frac{x_{23}}{\varepsilon}\right)^{2\hat{\Delta}} \left(\frac{x_{24}}{\varepsilon}\right)^{2\hat{\Delta}_4}}. \quad (104)$$

This is nothing but the tree level result (98) of the gauge theory.

7 Discussion and future directions

In this paper, we have computed the AdS part of the four point function for heavy scalar operators in $\mathcal{N} = 4$ SYM in the classical limit. For the particular case of BPS operators on a line with a single scalar field, the sphere part is known and thus we can construct the full strong coupling four point function.

The main ingredient of our method is the integrability of the string equations of motion in AdS_2 . Specifically, we use the method of Pohlmeyer reduction to map the problem to that of solving a certain modified Sinh-Gordon equation which is known to be integrable. We construct the linear problem associated with this equation, which has the form of an $SU(2)$ Hitchin system. This approach was used in the solution of the Null Polygonal Wilson-Loop problem at strong coupling [10] as well as in the study of three-point functions of heavy operators at strong coupling [8, 9, 11].

Let us mention that while our approach was inspired by these previous works, to solve the $N > 3$ point function problem required significant generalization of [10, 8, 9] as well as nontrivial new ingredients. For the case of the Null-Polygonal Wilson loop the world-sheet has the topology of a disk, whereas in our problem it is that of an N -punctured sphere and this changes the boundary conditions that one imposes. This issue was addressed in [8, 9] for the case of the 3-punctured sphere, however in those works the total monodromy condition was enough to derive the functional equations that determine the necessary objects. These functional equations are linear and can be easily inverted using standard techniques. For the case of 4 or more punctures the situation becomes significantly more complex. First of all, the total monodromy condition no longer provides enough information to fix the necessary objects. We have made heavy use of the formalism developed in [12] to derive the functional equations. Second, the inversion of these functional equations is more subtle due to their complexity. The result turns out to be some integral equations resembling the usual TBA equations.

Perhaps the most exciting aspect of this work is the multitude of interesting applications and extensions of the results. Let us consider each of these in turn.

- *Multiple configurations and phase transitions.* An important physical outcome of this paper is the emergence of multiple string configurations in AdS_2 . Each of these configurations is associated to the existence of several saddle points. A natural question is to figure out whether the dominant saddle point depends on the parameters of the theory. If so it would be interesting to study the phase diagram and the possible transitions. We have already made some preliminary progress in this direction and we hope to make a more extensive study in a future publication.
- *OPE.* A natural question to ask given any 4-point function in a conformal field theory is what can be learned from its OPE decomposition. In particular, important information about the spectrum and structure constants of the theory can be extracted.
- *GKP string.* An interesting aspect of [8, 9] is the similarity between the mathematical formalism employed despite the differences in the physical problem: [8] describes strings without spin in AdS_2 whereas [9] describes spinning strings in AdS_3 . In the formalism of [9, 11], one expresses the N -point function of GKP string in terms of a universal AdS contribution and a contribution from vertex operators, both of which can be computed for the case of the three-point function. It is possible that one could use the formalism developed in this work to calculate the AdS contribution to the N -point function of GKP strings.
- *N -point functions.* The formalism developed here does not depend in any special way on having only 4 punctures and in principle one could use the same methods to study the N -punctured sphere for any N . It would be interesting to understand how the functional equations generalize to higher N . Furthermore, since for the N -point function there will be $N - 3$ unfixed insertion points, the moduli space of possible configurations should be quite interesting.
- *TBA equations.* We should note that the techniques developed in [12], in principle, allow one to write the functional equations derived in this paper in the usual form of a Y-system. Typically this Y-system will involve an infinite number of Y-functions. This form of the equations could be useful for various applications including analytic continuation of parameters and generalization to N -point functions.
- *Generalizing out of the line and WL/CF duality* A natural step would be to generalize this work for operators not inserted on a line. In this case the string is embedded in a higher dimensional AdS space, which involves a more complicated Pohlmeyer reduction scheme. It would be interesting to study the question of whether the multiple string configurations/ saddle points we have found is special to AdS_2 case. Another promising application of such generalization would be the possibility of studying the OPE for the Null Polygonal Wilson Loop [22]-[24]. One could also investigate the duality between Null Polygonal Wilson Loops and Correlation functions of null separated local operators at strong coupling [25]-[30].

Many of these points present interesting opportunities to try to learn about finite coupling and weak/strong coupling interpolation and this is probably the most stimulating reason for pursuing them.

Acknowledgments

We thank Pedro Vieira for numerous invaluable discussions, motivation and inspiration throughout this work. We also thank Jorge Escobedo, Davide Gaiotto, Kolya Gromov, Romuald Janik, Amit Sever, Kostya Zarembo and Miguel Zilhão for many useful discussions. Finally, we thank Davide Gaiotto for valuable comments on the first version of this paper. JC is funded by the FCT fellowship SFRH/BD/69084/2010. This work has been supported in part by the Province of Ontario through ERA grant ER 06-02-293. Research at the Perimeter Institute is supported in part by the Government of Canada through NSERC and by the Province of Ontario through MRI. This work was partially funded by the research grants PTDC/FIS/099293/2008 and CERN/FP/116358/2010 and by Fund. Calouste Gulbenkian. *Centro de Física do Porto* is partially funded by FCT under grant PEst-OE/FIS/UI0044/2011.

A The linear problem

A.1 Summary of the linear problem

The linear problem associated with (10) is given by

$$(\partial + J_w) \psi = 0, \quad (\bar{\partial} + J_{\bar{w}}) \psi = 0 \quad (105)$$

where the connection has the form

$$J_w = \frac{1}{\xi} \Phi_w + A_w, \quad J_{\bar{w}} = \xi \Phi_{\bar{w}} + A_{\bar{w}} \quad (106)$$

$$\Phi_w = \begin{pmatrix} 0 & -\frac{1}{2}e^{\tilde{\gamma}} \\ -\frac{1}{2}Te^{-\tilde{\gamma}} & 0 \end{pmatrix} \quad (107)$$

$$\Phi_{\bar{w}} = \begin{pmatrix} 0 & -\frac{1}{2}\bar{T}e^{-\tilde{\gamma}} \\ -\frac{1}{2}e^{\tilde{\gamma}} & 0 \end{pmatrix} \quad (108)$$

$$A_w = \partial_w \begin{pmatrix} \frac{1}{2}\tilde{\gamma} & 0 \\ 0 & -\frac{1}{2}\tilde{\gamma} \end{pmatrix} \quad (109)$$

$$A_{\bar{w}} = \partial_{\bar{w}} \begin{pmatrix} -\frac{1}{2}\tilde{\gamma} & 0 \\ 0 & \frac{1}{2}\tilde{\gamma} \end{pmatrix} \quad (110)$$

For compactness we have introduced the combination $\tilde{\gamma} = 1/2(\gamma + \log \sqrt{T\bar{T}})$. The function γ is defined as the solution of the following problem

$$\begin{aligned}\partial\bar{\partial}\gamma &= \sqrt{T\bar{T}} \sinh \gamma \\ \gamma &\rightarrow \pm \frac{1}{2} \log T\bar{T} \quad (w \rightarrow z_a) \\ \gamma &\rightarrow 0 \quad (w \rightarrow w_a)\end{aligned}\tag{111}$$

where z_a and w_a are the zeros and the poles of T , respectively.

For the near-puncture analysis as well as the WKB analysis it is useful to make the field redefinition $\psi \rightarrow \hat{\psi} = \hat{G}\psi$ where

$$\hat{G} = \frac{1}{2} \begin{pmatrix} +e^{-\gamma/2} T^{1/4} \bar{T}^{-1/4} & 1 \\ -e^{-\gamma/2} T^{1/4} \bar{T}^{-1/4} & 1 \end{pmatrix}\tag{112}$$

This is usually referred to as ‘diagonal gauge’ in the literature. In diagonal gauge we have

$$\hat{\Phi}_w = \frac{1}{2} \sqrt{T} \begin{pmatrix} -1 & 0 \\ 0 & 1 \end{pmatrix}\tag{113}$$

$$\hat{\Phi}_{\bar{w}} = \frac{1}{2} \sqrt{\bar{T}} \begin{pmatrix} -\cosh \gamma & \sinh \gamma \\ -\sinh \gamma & \cosh \gamma \end{pmatrix}\tag{114}$$

$$\hat{A}_w = \partial_w \begin{pmatrix} \frac{1}{4}\gamma - \frac{1}{8} \log(T\bar{T}) & -\frac{1}{2}\gamma \\ -\frac{1}{2}\gamma & \frac{1}{4}\gamma - \frac{1}{8} \log(T\bar{T}) \end{pmatrix}\tag{115}$$

$$\hat{A}_{\bar{w}} = \partial_{\bar{w}} \begin{pmatrix} \frac{1}{4}\gamma + \frac{1}{8} \log(T\bar{T}) & 0 \\ 0 & \frac{1}{4}\gamma + \frac{1}{8} \log(T\bar{T}) \end{pmatrix}\tag{116}$$

We are now ready to consider the behavior of the solutions near the points w_a and z_a .

A.2 Solutions near w_a

Let us first consider the solutions of the linear problem in the neighborhood of one of the punctures. From (111) and the explicit expressions for $\hat{\Phi}$ and \hat{A} for $w \rightarrow w_a$ we have

$$\hat{\Phi}_w \rightarrow \frac{1}{2} \sqrt{T} \begin{pmatrix} -1 & 0 \\ 0 & +1 \end{pmatrix}, \quad \hat{\Phi}_{\bar{w}} \rightarrow \frac{1}{2} \sqrt{\bar{T}} \begin{pmatrix} -1 & 0 \\ 0 & +1 \end{pmatrix}\tag{117}$$

$$\hat{A}_w \rightarrow \partial_w \left(-\frac{1}{8} \log T\bar{T} \right) \begin{pmatrix} +1 & 0 \\ 0 & +1 \end{pmatrix}, \quad \hat{A}_{\bar{w}} \rightarrow \partial_{\bar{w}} \left(\frac{1}{8} \log T\bar{T} \right) \begin{pmatrix} +1 & 0 \\ 0 & +1 \end{pmatrix}\tag{118}$$

Then the solution in the vicinity of puncture P_a is given by:

$$\hat{\psi}^{\pm}(w) \equiv (T/\bar{T})^{1/8} e^{\pm \frac{1}{2} \int^w \xi^{-1} \omega + \xi \bar{\omega}} |\pm\rangle \sim (w - w_a)^{\pm \frac{1}{4} \Delta_a \xi^{-1} - \frac{1}{4}} (\bar{w} - \bar{w}_a)^{\pm \frac{1}{4} \bar{\Delta}_a \xi + \frac{1}{4}} |\pm\rangle\tag{119}$$

where $|\pm\rangle$ are the eigenvectors of the Pauli matrix σ^3 . Note the characteristic monodromy of the solutions about w_a .

A.3 Solutions near z_a

Now we will consider the behavior of the solutions near the zeros z_a of T . Notice from (107) - (110) and (111) that the connection is regular or singular at z_a depending on the direction of the spike in γ at z_a . More specifically, the connection is regular if $\gamma \sim -\log|w - z_a|$ and thus the solution will be regular in the vicinity of a d -spike. However, the connection has a singularity if $\gamma \sim +\log|w - z_a|$ and at the u -spikes one can check that in gauge (107) - (110) there are two linearly independent solutions behaving as

$$\Psi \sim \Psi_{z_a} \equiv \begin{pmatrix} (w-z_a)^{-1/4}(\bar{w}-\bar{z}_a)^{+1/4} & 0 \\ 0 & (w-z_a)^{+1/4}(\bar{w}-\bar{z}_a)^{-1/4} \end{pmatrix} \quad (120)$$

where we have written the two solutions in matrix form as in (71). Notice that Ψ has square-root type singularity at z_a since it has a monodromy of $\Psi \rightarrow (-1)\Psi$ about z_a . The solutions associated with the punctures $\{s_P\}$ and $\{\tilde{s}_P\}$ inherit this square-root singularity as one can see by expanding them in the basis (120) near z_a .

In our analysis it is crucial to account for the additional monodromies originating from u -spikes. Let us explain our conventions for doing this. If there is a u -spike at z_a , one can always make the gauge-transformation $\Psi \rightarrow \Psi_{z_a}^{-1}\Psi$ that removes the square root singularity (Ψ_{z_a} is given in (120)). Of course this gauge transformation contains the same multivaluedness and one must still account for it at the end of the day. In the main text we use the point of view that this gauge transformation has been performed for each u -spike. The connection in this gauge will only have singularities at the punctures and the solutions in this gauge will only have non-trivial monodromies around the punctures. In this way we can define small solutions that are single valued throughout some Q_E , as is the prescription of [12]. We must then be sure to account for the multivaluedness of these gauge transformations whenever we have a holonomy that encloses an odd number of u -spikes. Such holonomies arise in the WKB expansion of the coordinates and we will return to this issue below.

B WKB analysis

B.1 Statement of the WKB approximation

As we have discussed above, it is essential to have control over the $\xi \rightarrow 0, \infty$ asymptotics of the inner products. It is clear from (105 - 106) that these are both singular limits, and the basic idea of extracting this singularity is as follows. As discussed above, we have good control over the solutions in the neighborhood of the punctures. Thus what we would like to study is the transport

$$\text{Pexp} \left[- \int_{\mathcal{C}(w'_a \rightarrow w)} \frac{1}{\xi} \Phi + A + \xi \bar{\Phi} \right] \psi(w'_a) \quad (121)$$

where $\mathcal{C}(w'_a \rightarrow w)$ is a curve starting at w'_a , a point in the neighborhood of w_a , and terminating at a generic point w . Note that at any point on the punctured sphere C the Higgs

field Φ has the two eigenvalues $\mp\omega/2 = \mp\sqrt{T}/2 dw$ (which are single valued on the double cover $\tilde{\Sigma}$), and thus we can choose a gauge along \mathcal{C} where Φ is diagonal and given by

$$\Phi = \frac{1}{2} \begin{pmatrix} -\omega & 0 \\ 0 & \omega \end{pmatrix} \quad (122)$$

Now consider the $\xi \rightarrow 0$ limit. First consider an infinitesimal segment of \mathcal{C} in the neighborhood of P_a . In the neighborhood of P_a the connection (in diagonal gauge) becomes diagonal (see (117)-(118)) and thus one can break apart the path-ordered exponential. In particular, one can isolate the singular part $e^{-\int \Phi/\xi} |\pm\rangle$ which will have one component growing exponentially and one component decaying. Let us choose the branch of Φ such that the $|+\rangle$ component is the one that is growing as we transport along \mathcal{C} *away* from P_a (although for the moment we are still working in a neighborhood of P_a). This will correspond to the small solution at P_a since it is exponentially decaying as it is transported *toward* from P_a . The *WKB approximation* is the statement that the exponentially growing part of the solution as $\xi \rightarrow 0$ will continue to be given by $e^{-\int \Phi/\xi} |+\rangle$ as we transport away from the neighborhood of P_a (now leaving the neighborhood of P_a) as long as we follow a curve such that at every point we have

$$\text{Re}(\omega/\xi) > 0 \quad (123)$$

This condition is satisfied most strongly along a curve such that

$$\text{Im}(\omega/\xi) = 0 \quad (124)$$

Condition (123) is called the *WKB condition* and curves satisfying (124) are called *WKB curves* [12]. Along a WKB curve defined for $\text{Arg}(\xi) = \theta$ the WKB condition is satisfied for $\text{Arg}(\xi) \in (\theta - \pi/2, \theta + \pi/2)$ and the WKB approximation is guaranteed to hold in this range. For example, suppose there is a WKB line connecting P_a to P_b for $\theta \in (\theta_-, \theta_+)$ but not outside that range. Then the WKB approximation will reliably give the $\xi \rightarrow 0, \infty$ asymptotic for $\theta \in (\theta_- - \pi/2, \theta_+ + \pi/2)$. These statements are proven in [12] and we refer the reader there for a more detailed discussion.

B.2 Subleading WKB

We will now consider the $\xi \rightarrow 0$ limit of the inner products (or Wronskians) $(s_b \wedge s_a)(\xi)$. We consider the case when P_a and P_b are connected by a WKB line which will be an edge E_{ab} in the WKB triangulation. From the analysis of A.2 we know s_a and s_b in the neighborhood of P_a and P_b respectively. In order to evaluate the Wronskian we need to know the solutions at a common point. The approach here is to use the connection to transport the solution s_a along E_{ab} to a point w'_b in the neighborhood of P_b and then to evaluate the Wronskian at w'_b . That is, we want to study the $\xi \rightarrow 0$ behavior of

$$\langle s_b | \text{Pexp} \left[- \int_0^1 dt \frac{1}{\xi} H_0 + V \right] | s_a \rangle \quad (125)$$

where we defined

$$H_0 = \dot{w} \hat{\Phi}_w, \quad V = \dot{w} \hat{A}_w + \dot{\bar{w}} \hat{A}_{\bar{w}} + \xi \dot{\bar{w}} \hat{\Phi}_{\bar{w}} \quad (126)$$

The contour of integration in (125) is the edge E_{ab} and the components of (126) are defined in appendix A. The basic idea of the computation is to expand in a perturbative series where $\xi^{-1}H_0$ acts as the free Hamiltonian. Such a procedure will be valid so long as the free part of the Hamiltonian is sufficiently larger than V for all points along the curve, which will be true along the edges of the WKB triangulation. Then we can expand (125) in the Born series

$$(-1)\hat{\psi}_b^-\hat{\psi}_a^+\left(\langle+|e^{-\int_0^1 H_0/\xi}|+\rangle - \int_0^1 dt_1 \langle+|e^{-\int_{t_1}^1 H_0/\xi} V(t_1) e^{-\int_0^{t_1} H_0/\xi}|+\rangle\right. \\ \left. + \int_0^1 dt_2 \int_0^{t_2} dt_1 \langle+|e^{-\int_{t_1}^{t_2} H_0/\xi} V(t_2) e^{-\int_{t_1}^{t_2} H_0/\xi} V(t_1) e^{-\int_0^{t_1} H_0/\xi}|+\rangle\right) \quad (127)$$

Let us explain a subtle point regarding the ‘external states’ in the above expression. We start with the small solution at P_a which we take to be ψ_a^+ . We then transport it to P_b and then extract the coefficient of the exponentially growing part – that is, we take the inner product with the small part of this transported solution. Since $\psi_a^+ \sim |+\rangle$ grows as we transport it along a WKB curve (i.e. it decays as one follows the curve into P_a and thus grows as we transport it away from P_a) and H_0 is diagonal, we infer that the small part of the solution at P_b is the solution proportional to $|-\rangle$. Thus we take the out-state to be $\langle-|\psi_b^-$. Finally, since the inner product is the antisymmetric the $\langle-|$ gets flipped to a $\langle+|$.

Using the fact that $|\pm\rangle$ are eigenstates of the free Hamiltonian we can easily evaluate the order $\mathcal{O}(V^0)$ and $\mathcal{O}(V^1)$ terms in (127). For the $\mathcal{O}(V^2)$ term, we insert the identity $|+\rangle\langle+| + |-\rangle\langle-|$ between the two insertions of V . We find

$$(-1)\hat{\psi}_b^-\hat{\psi}_a^+ e^{+\frac{1}{2}\int_0^1 \omega/\xi} \left(1 - \int_0^1 dt_1 \langle+|V(t_1)|+\rangle + \frac{1}{2} \left[\int_0^1 dt_1 \langle+|V(t_1)|+\rangle \right]^2 + \right. \\ \left. \int_0^1 dt_2 \int_0^{t_2} dt_1 e^{-\int_{t_1}^{t_2} \omega/\xi} \langle+|V(t_2)|-\rangle \langle-|V(t_1)|+\rangle \right) \quad (128)$$

Now concentrate on the second term on the $\mathcal{O}(V^2)$ contribution. As $\xi \rightarrow 0$ the factor $\exp\left(-\int_{t_1}^{t_2} \omega/\xi\right)$ will suppress the integrand except for the small range $t_2 = t_1 + \mathcal{O}(\xi)$ and thus the result of the first integration will already be $\mathcal{O}(\xi)$. So to order ξ we can take ω to be constant and $V(t_1) \rightarrow V(t_2)$. We then find for the second term in the $\mathcal{O}(V^2)$ contribution

$$e^{\frac{1}{2}\int_0^1 \omega/\xi} \int_0^1 dt_2 \xi \frac{|\langle+|V(t_2)|-\rangle|^2}{\dot{w}\sqrt{T}} \quad (129)$$

Putting everything together, we see that the result re-exponentiates and we find

$$(-1)\hat{\psi}_b^-\hat{\psi}_a^+ \exp \left[+\frac{1}{\xi} \int_0^1 dt \frac{1}{2}\sqrt{T} - \int_0^1 dt \langle+|V(t)|+\rangle + \xi \int_0^1 dt \frac{|\langle+|V(t)|-\rangle|^2}{\dot{w}\sqrt{T}} \right] \quad (130)$$

Grouping each term based on its order in ξ (including the prefactors $\hat{\psi}_b^-\hat{\psi}_a^+$ whose explicit expression are given in (119)) we find

$$(s_b \wedge s_a)(\xi) \sim \exp \left[+\frac{1}{2}\xi^{-1}\varpi_{ab} + \alpha_{ab} + \frac{1}{2}\xi\overline{\varpi}_{ab} + \xi\eta_{ab} \right] \quad (131)$$

where

$$\varpi_{ab} = \lim_{w'_a \rightarrow w_a} \lim_{w'_b \rightarrow w_b} \left[\int_{E_{ab}} \sqrt{T} dw + \frac{\Delta_a}{2} \log(w_a - w'_a) + \frac{\Delta_b}{2} \log(w_b - w'_b) \right] \quad (132)$$

$$\alpha_{ab} = - \int_{E_{ab}} \left(\frac{1}{4} \partial_w \left(\gamma - \log \sqrt{T\bar{T}} \right) dw + \frac{1}{4} \partial_{\bar{w}} \left(\gamma + \log \sqrt{T\bar{T}} \right) d\bar{w} \right) \quad (133)$$

$$\eta_{ab} = \int_{E_{ab}} \left(\frac{1}{2} \sqrt{\bar{T}} (\cosh \gamma - 1) d\bar{w} + \frac{1}{4\sqrt{T}} (\partial\gamma)^2 dw \right) \quad (134)$$

This completes the derivation of formula (26) used in the main text. The integral ϖ_{ab} is defined as in (58). Note that the logarithmic terms in ϖ_{ab} in (131) are due to the prefactor $\hat{\psi}_b^- \hat{\psi}_a^+$. These terms precisely cancel the singularities at the endpoints of the integral $\int_a^b \omega$ so that ϖ_{ab} is finite as we continue the limits of integration all the way up to punctures at w_a and w_b [8].

B.3 WKB expansion of the coordinates

In the previous section we derived the $\xi \rightarrow 0$ WKB expansion of $(s_a \wedge s_b)$ up to order $\mathcal{O}(\xi)$. To compute the WKB expansion of the coordinate χ_E we simply combine the expansions for each edge of the quadrilateral Q_E , taking care to account for the directions of the WKB lines as discussed in section 4.6. When this is done each of the integrals (132) - (134) become closed integrals along the cycle γ_E . The asymptotics of the χ -functions are needed for the inversion of the χ -system described in section 4.9. For that purpose only the non-vanishing contributions are needed in the $\xi \rightarrow 0, \infty$ limits.

There is one very important subtlety that must be addressed here, which is that of the monodromy around u -spikes discussed in appendix A.3. We take the point of view that we have made the (multi-valued) gauge-transformation (120) that removes the monodromy about each u -spike. The small solutions in this gauge are single valued throughout Q_E , but we must account for the monodromy of the gauge transformation about Q_E . This monodromy is simply $(-1)^{u_E}$ where u_E is the number of u -spikes in Q_E .

Combining the above discussion with (133), the constant term in the WKB expansion of χ_E is given by

$$C_E^{(0)} = \log(-1)^{u_E} - \frac{1}{4} \int_{\gamma_E} \left(d\gamma + *d \log \sqrt{T\bar{T}} \right) = \log(-1)^{u_E} \pm i\pi \quad (135)$$

To arrive at the last equality (135) we have used the fact that γ is single-valued on the 4-punctured sphere so that the integral of $d\gamma$ on any closed contour is zero. The integral of $*d \log \sqrt{T\bar{T}}$ is simple to do explicitly and gives the $\pm i\pi$ factor.³⁰

The discussion of the $\xi \rightarrow \infty$ limit follows along the same lines as the $\xi \rightarrow 0$ limit.

³⁰The \pm depends on the orientation of γ_E but both signs have the same overall effect so that the \pm is irrelevant.

The singular term is given by $e^{\xi \int_{\gamma_E} \bar{\omega}/2}$. The constant term is the same. Thus the full non-vanishing WKB asymptotic is given by

$$\chi_E \sim (-1)^{u_E} \exp \left[\frac{1}{2} \int_{\gamma_E} (\xi^{-1} \omega + \xi \bar{\omega}) \right] \quad (136)$$

where we recall that u_E is the number of u -spikes enclosed in γ_E . This is the expression (40) used in the main text.

C Fold lines and Properties of γ

In this appendix we discuss some properties of the function γ and how they are related to geometric features of the string embedding. In appendix C.1 we show that the world-sheet contours where $\gamma = 0$ map to the fold-lines of the target space solution; in appendix C.2 we discuss how the geometry of the string embedding near the boundary is deduced from the structure of these $\gamma = 0$ contours near the points w_a ; finally, in section C.3 we show how the global structure of the $\gamma = 0$ contours is deduced from the choice of spikes in γ . The point of this appendix is to give the background details that were omitted in the discussion of section 3.3.

C.1 Fold lines

In this section we show that the contours on the worldsheet where $\gamma = 0$ map to the fold lines of the string embedding. This was pointed out in [8]. Recall the relation between γ and the world-sheet metric

$$\sqrt{T\bar{T}} \cosh \gamma = \frac{\partial x \bar{\partial} x + \partial z \bar{\partial} z}{z^2} \quad (137)$$

Furthermore, we have

$$T(w) = \frac{(\partial x)^2 + (\partial z)^2}{z^2}, \quad \bar{T}(\bar{w}) = \frac{(\bar{\partial} x)^2 + (\bar{\partial} z)^2}{z^2} \quad (138)$$

Now, suppose that \mathcal{C} is a curve on the worldsheet that maps to a fold-line of the string and consider a point \mathcal{P} in that curve. We can choose local coordinates at \mathcal{P} so that the derivative takes the form $\partial_w \rightarrow e^{i\phi} (\partial_t + i\partial_n)$ where the direction ∂_n is chosen such that $\partial_n z = 0$. The prefactor $e^{i\phi}$ is the Jacobian of the coordinate transformation (just a translation and rotation). The defining property of the fold-line is then that the x -coordinate reaches a local extrema and thus we also have $\partial_n x = 0$ as we cross the fold. Therefore along the fold-line we have (with $\partial_t x = \dot{x}$)

$$\sqrt{T\bar{T}} \cosh \gamma \rightarrow \frac{\dot{x}^2 + \dot{z}^2}{z^2}, \quad T(w) \rightarrow e^{2i\phi} \frac{\dot{x}^2 + \dot{z}^2}{z^2}, \quad \bar{T}(\bar{w}) \rightarrow e^{-2i\phi} \frac{\dot{x}^2 + \dot{z}^2}{z^2} \quad (139)$$

Using the last two equations to solve for $\sqrt{T\bar{T}}$ we see that they are consistent with the first equation only if $\gamma = 0$. Therefore, the worldsheet contours where $\gamma = 0$ map to the fold-lines of the string-embedding. For this reason, we frequently refer to the contours where $\gamma = 0$ as fold-lines.

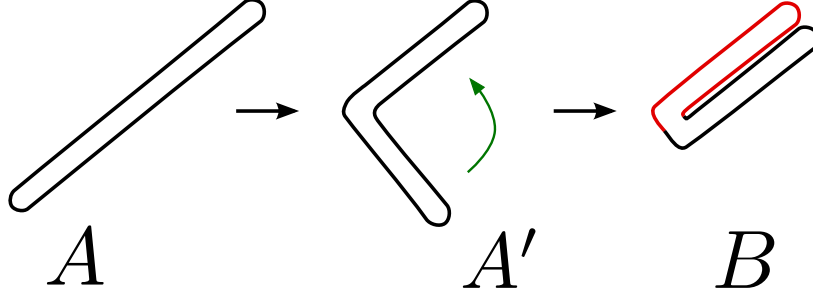


Figure 19: Single-folded and double-folded string in panels A and B respectively.

C.2 Structure of γ near w_a

To gain some intuition about the structure of the contours where $\gamma = 0$ it is useful to study the behavior of γ near the points w_a . Recall that γ is defined as the solution to the PDE:

$$\partial\bar{\partial}\gamma = \sqrt{T\bar{T}} \sinh \gamma \quad (140)$$

subject to the boundary conditions

$$\gamma \rightarrow \pm \frac{1}{2} \log T\bar{T} \quad (w \rightarrow z_a) \quad (141)$$

$$\gamma \rightarrow 0 \quad (w \rightarrow P_a) \quad (142)$$

The boundary condition (142) simply imposes that γ is non-singular at the singularities of T and this condition is automatically imposed if we demand the solution be regular away from the zeros of T .

Since we know that γ must vanish at singularities of T , it's natural to study the function in the neighborhood of these points. Let us consider some P_a and use polar coordinates (r, ϕ) in which the origin is at w_a . Since γ is vanishing, we can linearize the RHS of (140). Further, we can take $\sqrt{T\bar{T}} \sim |\Delta|^2/(4r^2)$. The PDE becomes linear and separable and using standard techniques one finds the series solution

$$\gamma \sim g_0 r^{\frac{1}{2}\Delta} + \sum_{m=1}^{\infty} g_m \sin(m\phi + \delta_m) r^{\frac{1}{2}\sqrt{\Delta^2+4m^2}} \quad (143)$$

Now consider a small circle centered at $r = 0$. As $r \rightarrow 0$ the series (143) is dominated by the lowest mode in the expansion. Thus along an infinitesimal circle centered at $r = 0$ the series (143) will vanish $2m^*$ times, where g_{m^*} is the smallest non-zero coefficient g_m , $m = 0, 1, 2, \dots$ in the series. Thus, if g_0 is the smallest non-zero coefficient then the series will vanish only at the point w_a which will be a local extrema. If $m^* = 1$ then the series will vanish along a single curve passing through P_a ; if $m^* = 2$ then γ will vanish along two curves that intersect at P_a , and so on.

The fact that the contours where $\gamma = 0$ map to fold-lines of the target-space solution gives a clear geometric meaning to each possible behavior $m^* = 1, 2, \dots$ near an insertion

point. For $m^* = 1$ we will cross two fold-lines as the world-sheet coordinate traverses a small loop around the point w_a . This means that near the insertion point the string is single-folded as shown in figure 19A. For $m^* = 2$ we will cross two fold-lines as the world-sheet coordinate traverses a small loop around the point w_a . This means that near the insertion point the string is double-folded as shown in figure 19B, for example. In general for $n > 0$ the case $m^* = n$ should correspond to an n -folded string. The only subtle case seems to be $m^* = 0$. Apparently if $m^* = 0$, as we traverse a closed loop around w_a the contour swept out in the target space does not close since there is no point at which the coordinates (x, z) can ‘turn around’. In this paper we are only interested in solutions that are closed (i.e. the embedding coordinates have trivial monodromies around operator the insertion points x_a) and thus we will only study cases for which $m^* > 0$ at all w_a . This is further discussed in appendix C.3.

It is important to keep in mind that (as we mentioned above) the behavior of γ at P_a is not our choice, and is determined by regularity and the conditions (141). In other words, for fixed T the only remaining conditions one can specify are the choice of signs in (141). For each choice of signs there will be a unique m^* for each P_a . In the next section we demonstrate how this works using the T of the 4-point function discussed in the main text.

C.3 Structure of contours where $\gamma = 0$

In this section we describe why the spike configurations of figure 4 are the only two physically relevant configurations. Furthermore, we deduce the structure of the contours where $\gamma = 0$ for each of these spike configurations.

Consider T fixed to be that of the 4-point function discussed in the main text (see equation (60) and figure 15). There are 4 zeros and therefore 2^4 ways to choose the signs in (141). Because of the symmetry of (140) under $\gamma \rightarrow -\gamma$, without loss of generality we can fix one of the spikes to be up which leaves 2^3 choices. Now, because the string is embedded in AdS_2 we know that it must be folded. Moreover we know that the operator insertions x_a will sit along the fold-lines of the target-space solution. In the world-sheet coordinates this translates to the statement that we should require $m^* > 0$ at each w_a . That is, there should be at least one contour where $\gamma = 0$ running through each insertion point w_a . For the 4-point function T (see equation (60) and figure 15) the only obvious way to accomplish this in general is to choose the spikes such that $\gamma \rightarrow -\gamma$ under reflection about the real axis. This leaves only the spike configurations of figure 20A,B, which are those of figure 4 used in the main text. We will now discuss the global structure of the $\gamma = 0$ contours for these two choices of spikes.

In figure 20 we show the fold-structure for three different spike configurations. The black lines schematically represent the contours where $\gamma = 0$ and one can read off the m^* associated with each puncture. The structure of these contours is determined purely by the choice of the directions of the spikes of γ . We refer to these contours as ‘fold lines’ since they map onto the fold-lines of the target-space embedding (see appendix C.1). We guess the structure of the fold lines for each choice of the spikes as follows: u spikes must be separated from d spikes by at least one fold line; we use the minimum number of fold lines needed to

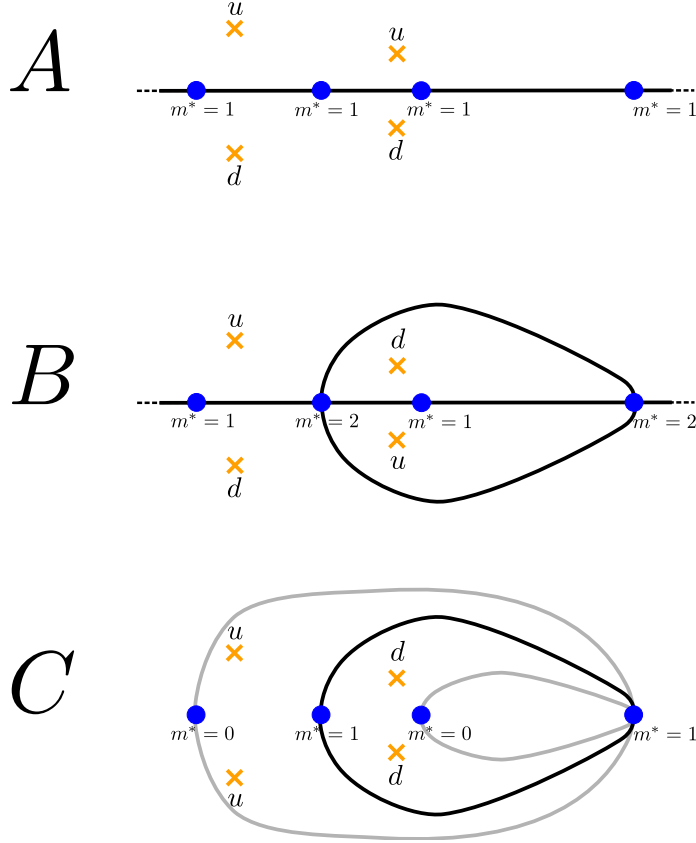


Figure 20: Three different spike configurations and the corresponding structure of the $\gamma = 0$ contours. The black lines schematically represent the contours where $\gamma = 0$ and one can read off the m^* associated with each puncture. Panels *A* and *B* show the physically relevant configurations studied in the main text. Panel *C* shows a third spike configuration which is not physical due to the presence of $m^* = 0$ behavior at two of the insertion points. The gray contours in panel *C* indicate contours that cannot correspond to fold-lines due to the restriction that $\gamma = 0$ contours must encircle at least one zero of T (see footnote 31). In this figure we are not indicating the location saddle-point w_4^* because it is not relevant for the present discussion (so long as it is located somewhere on the real axis).

accomplish this for all spikes. Note that fold lines must encircle at least one zero of T .³¹ This restriction is useful because, for example, it allows one to rule-out the possibility of fold-lines corresponding to the gray contours in figure 20C. This is important because if it was possible for the gray contours to be fold-lines then it might be possible to have a solutions with all $m^* > 0$ for configuration *C*. Configurations *A* and *B* are the physical configurations that

³¹ Consider a closed contour along which $\gamma = 0$ and suppose (for a contradiction) that it does not enclose any zeros of T . Let \mathcal{D} be the region enclosed by the contour. This contour must separate positive values from negative values (i.e. it cannot sit at the bottom of a ‘valley’ since this locally violates the equation (140)). Suppose for simplicity that $\gamma < 0$ in \mathcal{D} . Since γ is regular away from the zeros of T , there must be at least one local minimum inside \mathcal{D} , and therefore at least one point where $(\partial_x^2 + \partial_y^2)\gamma \geq 0$. Thus at such a point the LHS of (140) is positive or zero, but the RHS is strictly less than zero by assumption, which is the desired contradiction.

we study in this paper and we have checked the fold structures of figure 20A,B numerically. Configuration C is an example of a spike-configuration that does not correspond to a target-space solution with the desired properties; the corresponding fold structure is only our best guess but we have not checked it numerically.

To summarize this appendix, in appendix C.1 we showed that the world-sheet contours where $\gamma = 0$ map to the fold-lines of the target space solution; in appendix C.2 we discussed how the geometry of the string embedding near the boundary is deduced from the structure of these $\gamma = 0$ contours near the points w_a ; finally, in section C.3 we discussed how the global structure of the $\gamma = 0$ contours is deduced from the choice of spikes in γ . From all of this one can deduce some qualitative global features of the string embedding, which is discussed in detail in section 3.3.

D Details of the 4-point function computation

D.1 Explicit expression for stress-energy tensor coefficients

For completeness we present the coefficients c_a of the stress-energy tensor in formula (60),

$$\begin{aligned}
c_\infty &= \frac{\Delta_\infty^2}{4} \\
c_0 &= \frac{1}{4} [4Uw_4 + 2w_4(1+w_4)\Delta_3^2 + (-1+w_4)(2w_4\Delta_1^2 + (1+w_4)(\Delta_2^2 - \Delta_4^2))] \\
c_1 &= \frac{1}{2} [-2U + (-1+w_4)^2\Delta_1^2 - (1+w_4)^2\Delta_3^2] \\
c_2 &= \frac{1}{4} [-4Uw_4 + 2(1+w_4)\Delta_3^2 + (-1+w_4)(-2\Delta_1^2 + (1+w_4)(-\Delta_2^2 + \Delta_4^2))] \quad (144)
\end{aligned}$$

D.2 Explicit expressions for χ -functions and A_{PQ}

For reference, we include here the explicit expressions for the χ -functions for the triangulation of figure 15. They are given by

$$\chi_{12} = (-1) \frac{(s_1 \wedge M_1^{-1} s_4)(s_2 \wedge s_4)}{(M_1^{-1} s_4 \wedge s_2)(s_4 \wedge s_1)} \quad (145)$$

$$\chi_{23} = (-1) \frac{(s_2 \wedge M_3 s_4)(s_3 \wedge s_4)}{(M_3 s_4 \wedge s_3)(s_4 \wedge s_2)} \quad (146)$$

$$\chi_{34} = (-1) \frac{(s_4 \wedge s_2)(s_3 \wedge M_3^{-1} s_2)}{(s_2 \wedge s_3)(M_3^{-1} s_2 \wedge s_4)} \quad (147)$$

$$\chi_{14} = (-1) \frac{(s_4 \wedge M_1 s_2)(s_1 \wedge s_2)}{(M_1 s_2 \wedge s_1)(s_2 \wedge s_4)} \quad (148)$$

$$\chi_{24} = (-1) \frac{(s_2 \wedge s_3)(s_4 \wedge s_1)}{(s_3 \wedge s_4)(s_1 \wedge s_2)} \quad (149)$$

$$\chi_{\hat{2}4} = (-1) \frac{(M_3^{-1} s_2 \wedge M_4 s_1)(s_4 \wedge s_3)}{(M_4 s_1 \wedge s_4)(s_3 \wedge M_3^{-1} s_2)} \quad (150)$$

One can check that these coordinates satisfy the rule (37) at each puncture. The χ -system obeyed by these coordinates is given by

$$\chi_{24}\chi_{24}^{++} = \left(\chi_{\hat{2}4}\chi_{\hat{2}4}^{++}\right)^{-1} = \frac{(1+A_{23})(1+A_{14})}{(1+A_{34})(1+A_{12})} \quad (151)$$

$$\chi_{12}\chi_{12}^{++} = \left(\chi_{14}\chi_{14}^{++}\right)^{-1} = \chi_{34}\chi_{34}^{++} = \left(\chi_{23}\chi_{23}^{++}\right)^{-1} = \frac{(1+A_{24})}{(1+A_{\hat{2}4})} \quad (152)$$

where the A_{PQ} are given by

$$A_{12} = \frac{\chi_{12}(1+\chi_{14})(1+\hat{\chi}_{24}(1+\chi_{23}(1+\chi_{24})))}{(1-\mu_1^2)(1-\mu_2^2)} \quad (153)$$

$$A_{23} = \frac{\chi_{23}(1+\chi_{34})(1+\chi_{24}(1+\chi_{12}(1+\chi_{\hat{2}4})))}{(1-\mu_2^2)(1-\mu_3^2)} \quad (154)$$

$$A_{34} = \frac{\chi_{34}(1+\chi_{23})(1+\hat{\chi}_{24}(1+\chi_{14}(1+\chi_{24})))}{(1-\mu_3^2)(1-\mu_4^2)} \quad (155)$$

$$A_{14} = \frac{\chi_{14}(1+\chi_{12})(1+\chi_{24}(1+\chi_{34}(1+\hat{\chi}_{24})))}{(1-\mu_1^2)(1-\mu_4^2)} \quad (156)$$

$$A_{24} = \frac{\chi_{24}(1+\chi_{12}(1+\chi_{\hat{2}4}(1+\chi_{23}))) (1+\chi_{43}(1+\chi_{42}(1+\chi_{41})))}{(1-\mu_2^2)(1-\mu_4^2)} \quad (157)$$

$$A_{\hat{2}4} = \frac{\hat{\chi}_{24}(1+\chi_{23}(1+\chi_{24}(1+\chi_{12}))) (1+\chi_{41}(1+\chi_{42}(1+\chi_{43})))}{(1-\mu_2^2)(1-\mu_4^2)} \quad (158)$$

Using the explicit expressions for the coordinates (145)-(150), schouten identity and the shift relation (43) one can directly verify the functional equations (151)-(152).

D.3 Finite part of AdS

In this section, we present some intermediate steps in the derivation of our formula (66) for the finite part of the AdS contribution. We want to compute

$$A_{fin} = \frac{\pi}{3} - \frac{i}{2} \left(\oint_{\gamma_a} \omega \right) I_{ab}^{-1} \left(\oint_{\gamma_b} \eta \right). \quad (159)$$

according to the steps outline in section 5.1.3. The complete basis of five a-cycles and five b-cycles that we chose is depicted in figure 21. From this figure we also read-off the intersection

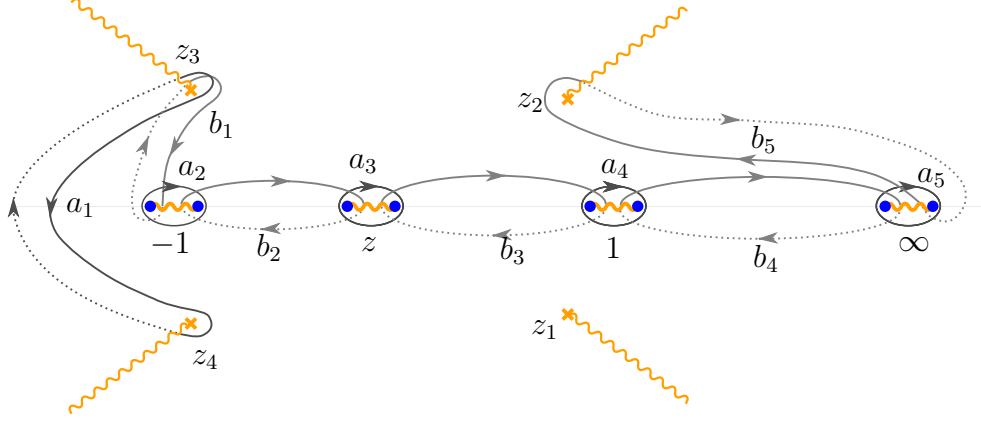


Figure 21: The cycles for Riemann bilinear identity. The dashed line represents a contour in a different Riemann sheet. The wavy lines represent a choice of branch cuts. From this picture we also read the intersection matrix I_{ab} of the cycles. For each pair of cycles, say γ_a and γ_b , intersecting at a point with tangent vectors ∂_a and ∂_b respectively, we assign $I_{ab} = +1$ (-1) if $\det [\{\partial_a, \partial_b\}] > 0$ (< 0).

matrix $I_{ab} = (\delta_{a+1,b} - \delta_{a-1,b})$ using the conventions described in the caption. The only other ingredient we need is

$$\int_{a_i} \eta = 0, \quad i = 2, \dots, 5 \quad (160)$$

which follows from the regularity of η at the poles of T . Plugging into (159) and computing we find

$$A_{fin} = \frac{\pi}{3} + i (\omega_{a_1} \eta_{z_3, z_2} + \omega_{a_2} \eta_{-1, z_2} + \omega_{a_3} \eta_{z, z_2} + \omega_{a_4} \eta_{1, z_2} + \omega_{a_5} \eta_{\infty, z_2}) - i \left(\sum_{i=1}^5 \omega_{b_i} \right) \eta_{z_3, z_4} \quad (161)$$

where we are using the notation $\eta_{ab} = \int_a^b \eta$ and $\omega_c = \int_c \omega$ and the contours are defined in figures 21 and 22.

Each of these η_{ab} can be written as a linear combination of the $\eta_{E_{ab}} = \int_{E_{ab}} \eta$ where the integral is taken along the WKB-line from P_a to P_b and the direction of the contour is the same as that of the WKB line. The idea is to combine the $\eta_{E_{ab}}$ to form the contour that we want. Let us exemplify with η_{1, z_2} . From the WKB configuration, see figure 22, we see that the large θ expansion of the ratio $\frac{(s_1 \wedge s_2)(s_1 \wedge s_4)}{(s_2 \wedge s_4)}$ involves a cycle that can be continuously deformed into *twice* the line integral connecting the puncture at $w = 1$ and the zero at $w = z_2$. Therefore we have

$$\eta_{1, z_2} = \frac{1}{2} \int_{-\infty}^{\infty} \frac{d\theta}{\pi} e^{-\theta} \log \left[\frac{(1 + A_{12}^-)(1 + A_{14}^-)}{(1 + A_{24}^-)} \right] = \frac{1}{2} (\eta_{E_{12}} + \eta_{E_{14}} - \eta_{E_{24}}) \quad (162)$$

In the same way we obtain

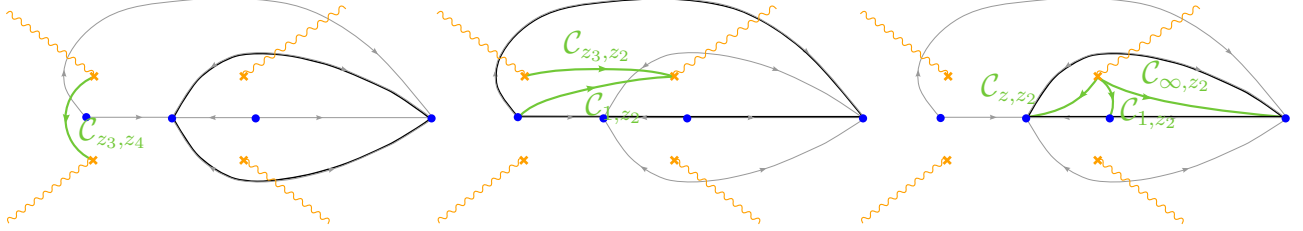


Figure 22: To extract line integrals connecting a zero to puncture or connecting two zeros we combine products of elementary solutions that have WKB expansions involving integrals over the paths indicated by the black lines. The resulting closed contours can be continuously deformed into the contour that we want, indicated by the green lines. The precise way of combining these products is dictated by the direction of the WKB lines indicated by the gray arrows.

$$\eta_{z_3, z_4} = \frac{1}{2} (\eta_{24} - \eta_{2\hat{4}}) \quad (163)$$

$$\eta_{-1, z_2} = \frac{1}{2} (2\eta_{34} + \eta_{12} - \eta_{14} - \eta_{24}) \quad (164)$$

$$\eta_{z, z_2} = \frac{1}{2} (\eta_{12} - \eta_{14} - \eta_{24}) \quad (165)$$

$$\eta_{\infty, z_2} = \frac{1}{2} (\eta_{14} - \eta_{12} - \eta_{24}) \quad (166)$$

$$\eta_{z_3, z_2} = \frac{1}{2} (\eta_{12} + \eta_{34} - \eta_{14} - \eta_{23}) \quad (167)$$

where the notation is the natural simplification of that used in (162). Plugging these expressions into (161) and re-collecting each η_E , one finds that the coefficient of η_E is simply ω_E where ω_E is the ω -cycle the intersects edge E , *not* the integral of ω along edge E (which would be divergent). That is, it's (1/2 of) the ω -cycle associated with the coordinate χ_E which are shown in figure 15. Thus we have

$$A_{fin} = \frac{\pi}{3} - i \sum_{E \in \mathcal{T}} \omega_E \eta_E \quad (168)$$

which is formula (66) as desired.

Equation (168) is perhaps the simplest possible result one could write from the triangulation data. Given this simplicity, it is probably possible to derive the result in a much more elegant way and perhaps even for any number of punctures. We have not pursued this issue but feel that it merits further exploration.

E Three-point function in GMN language

In this section we apply the method developed in section 4 to the three point correlation function studied in [8]. We use the setup of [8], namely the same stress-energy tensor. We aim at deriving a set of functional equations to extract the cycles used there.

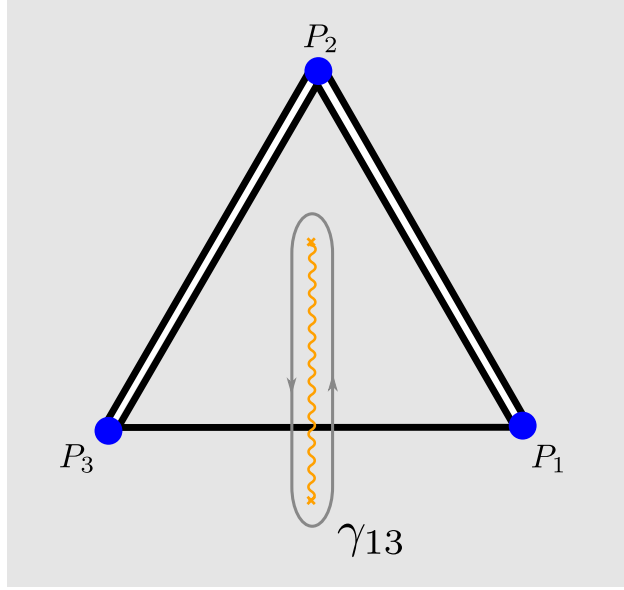


Figure 23: The WKB triangulation for the 3-point function is composed of 3 edges forming two triangles on the sphere. Here we show the construction of the coordinate χ_{13} . We are using the edge-splitting procedure discussed in section 4.5 (in particular, see figure 12). The gray contour shows the cycle associated with the coordinate χ_{13} .

As a starting point, we introduce the WKB triangulation for this configuration from which we define the coordinates, see figure 23. From this figure, we easily derive the χ -system. Since the quadrilateral is very degenerate it follows from (46) that the right hand side of the χ -system is equal to 1. The reason is that the same auxiliary A_{PQ} 's appear both in numerator and denominator canceling each other. Hence, the solution of the functional equations is simply given by the WKB asymptotics. More explicitly, the χ functions take the form

$$\chi_{ac} = (-1) \exp \left(\frac{1}{2} e^\theta \int_{\gamma_{ac}} \omega + \frac{1}{2} e^{-\theta} \int_{\gamma_{ac}} \bar{\omega} \right) = -\frac{\mu_a \mu_c}{\mu_b} \quad (169)$$

where a , b and c are distinct.³² The spikes must be in pointing in opposite direction as follows from the discussion of appendix C. This is the the origin of the (-1) prefactor in (169). The cycles of ω are given in terms of the dimensions of the operators,

$$\int_{\gamma_{ac}} \omega = i\pi(-\Delta_a - \Delta_c + \Delta_b) \quad (170)$$

Having the solutions of the functional equations, we can easily find the auxiliary quantities A_{PQ} using the rules of section 4.8. The determination of the η -cycles is also straightforward. To compare with the result in [8] let us set $\Delta_1 = \Delta_2 = \Delta$ and $\Delta_3 = \Delta_\infty$. We use expression

³²This result also follows directly from the definition of the coordinates in terms of the small solutions, $\chi_{ac} = -\frac{(s_c \wedge s_b)(s_a \wedge M_a^{-1} s_b)}{(M_a^{-1} s_b \wedge s_c)(s_b \wedge s_a)}$ for distinct a, b and c ; all the inner-products cancel and one is left with only the monodromy factors in (169).

57 to compute the cycles, and we get

$$\int_{-1}^1 \eta = \int_{\mathbb{R}} \frac{d\theta}{\pi} e^{-\theta} \log(1 + A_{12}^-) = h(2\Delta - \Delta_\infty) + h(2\Delta + \Delta_\infty) - 2h(2\Delta) \quad (171)$$

$$\int_1^\infty \eta = \int_{\mathbb{R}} \frac{d\theta}{\pi} e^{-\theta} \log(1 + A_{23}^-) = h(\Delta_\infty) + h(2\Delta + \Delta_\infty) - h(2\Delta) - h(2\Delta_\infty) \quad (172)$$

where we define

$$h(x) = \int_{\mathbb{R}} \frac{d\theta}{\pi} \cosh \theta \log(1 - e^{-x\pi \cosh \theta}) . \quad (173)$$

This is precisely the result obtained in [8]. A last comment about the expression for the area in the three point function. It is easy to show using the same type of manipulation of the four point function case that the area can be expressed in terms of elements of the WKB triangulation as

$$A_{fin} = \frac{\pi}{6} - i \sum_{E \in \mathcal{T}} \omega_E \eta_E \quad (174)$$

where the sum is over the edges of the triangulation of figure 23. As in the case of the four point function, we define $\eta_{E_{ab}}$ as the η -cycle that passes along edge E_{ab} from P_a to P_b and $\omega_{E_{ab}}$ as the ω -cycle that intersects edge E_{ab} .

References

- [1] J. M. Maldacena, “The Large N limit of superconformal field theories and supergravity,” *Adv. Theor. Math. Phys.* **2**, 231 (1998) [*Int. J. Theor. Phys.* **38**, 1113 (1999)] [arXiv:hep-th/9711200].
- [2] J. Escobedo, N. Gromov, A. Sever and P. Vieira, “Tailoring Three-Point Functions and Integrability II. Weak/strong coupling match,” *JHEP* **1109**, 029 (2011) [arXiv:1104.5501 [hep-th]].
- [3] J. Caetano and J. Escobedo, “On four-point functions and integrability in N=4 SYM: from weak to strong coupling,” *JHEP* **1109**, 080 (2011) [arXiv:1107.5580 [hep-th]].
- [4] N. Gromov, A. Sever and P. Vieira, “Tailoring Three-Point Functions and Integrability III. Classical Tunneling,” *JHEP* **1207**, 044 (2012) [arXiv:1111.2349 [hep-th]].
- [5] N. Gromov and P. Vieira, “Quantum Integrability for Three-Point Functions,” arXiv:1202.4103 [hep-th].
- [6] I. Kostov, “Three-point function of semiclassical states at weak coupling,” arXiv:1205.4412 [hep-th].
- [7] R. A. Janik, P. Surowka and A. Wereszczynski, “On correlation functions of operators dual to classical spinning string states,” *JHEP* **1005**, 030 (2010) [arXiv:1002.4613 [hep-th]].

- [8] R. A. Janik and A. Wereszczynski, “Correlation functions of three heavy operators: The AdS contribution,” JHEP **1112**, 095 (2011) [arXiv:1109.6262 [hep-th]].
- [9] Y. Kazama and S. Komatsu, “On holographic three point functions for GKP strings from integrability,” JHEP **1201**, 110 (2012) [Erratum-ibid. **1206**, 150 (2012)] [arXiv:1110.3949 [hep-th]].
- [10] L. F. Alday, J. Maldacena, A. Sever and P. Vieira, “Y-system for Scattering Amplitudes,” J. Phys. A **43**, 485401 (2010) [arXiv:1002.2459 [hep-th]].
- [11] Y. Kazama and S. Komatsu, “Wave functions and correlation functions for GKP strings from integrability,” arXiv:1205.6060 [hep-th].
- [12] D. Gaiotto, G. W. Moore and A. Neitzke, “Wall-crossing, Hitchin Systems, and the WKB Approximation,” arXiv:0907.3987 [hep-th].
- [13] A. M. Polyakov, “Gauge fields and space-time,” Int. J. Mod. Phys. A **17S1**, 119 (2002) [hep-th/0110196].
- [14] A. A. Tseytlin, “On semiclassical approximation and spinning string vertex operators in AdS(5) x S**5,” Nucl. Phys. B **664**, 247 (2003) [hep-th/0304139].
- [15] S. S. Gubser, I. R. Klebanov and A. M. Polyakov, “A Semiclassical limit of the gauge / string correspondence,” Nucl. Phys. B **636**, 99 (2002) [hep-th/0204051].
- [16] E. D’Hoker, D. Z. Freedman, S. D. Mathur, A. Matusis and L. Rastelli, “Extremal correlators in the AdS / CFT correspondence,” In *Shifman, M.A. (ed.): The many faces of the superworld* 332-360 [hep-th/9908160].
- [17] B. Eden, P. S. Howe, C. Schubert, E. Sokatchev and P. C. West, “Extremal correlators in four-dimensional SCFT,” Phys. Lett. B **472**, 323 (2000) [hep-th/9910150].
- [18] M. S. Costa, J. Penedones, D. Poland and S. Rychkov, “Spinning Conformal Blocks,” JHEP **1111**, 154 (2011) [arXiv:1109.6321 [hep-th]].
- [19] M. S. Costa, J. Penedones, D. Poland and S. Rychkov, “Spinning Conformal Correlators,” JHEP **1111**, 071 (2011) [arXiv:1107.3554 [hep-th]].
- [20] D. Simmons-Duffin, “Projectors, Shadows, and Conformal Blocks,” arXiv:1204.3894 [hep-th].
- [21] F. A. Dolan and H. Osborn, “Conformal partial waves and the operator product expansion,” Nucl. Phys. B **678**, 491 (2004) [hep-th/0309180].
- [22] L. F. Alday, D. Gaiotto, J. Maldacena, A. Sever and P. Vieira, “An Operator Product Expansion for Polygonal null Wilson Loops,” JHEP **1104**, 088 (2011) [arXiv:1006.2788 [hep-th]].
- [23] D. Gaiotto, J. Maldacena, A. Sever and P. Vieira, “Bootstrapping Null Polygon Wilson Loops,” JHEP **1103**, 092 (2011) [arXiv:1010.5009 [hep-th]].

- [24] D. Gaiotto, J. Maldacena, A. Sever and P. Vieira, “Pulling the straps of polygons,” JHEP **1112**, 011 (2011) [arXiv:1102.0062 [hep-th]].
- [25] L. F. Alday, B. Eden, G. P. Korchemsky, J. Maldacena and E. Sokatchev, “From correlation functions to Wilson loops,” JHEP **1109**, 123 (2011) [arXiv:1007.3243 [hep-th]].
- [26] B. Eden, G. P. Korchemsky and E. Sokatchev, “From correlation functions to scattering amplitudes,” JHEP **1112**, 002 (2011) [arXiv:1007.3246 [hep-th]].
- [27] B. Eden, G. P. Korchemsky and E. Sokatchev, “More on the duality correlators/amplitudes,” Phys. Lett. B **709**, 247 (2012) [arXiv:1009.2488 [hep-th]].
- [28] A. V. Belitsky, G. P. Korchemsky and E. Sokatchev, “Are scattering amplitudes dual to super Wilson loops?,” Nucl. Phys. B **855**, 333 (2012) [arXiv:1103.3008 [hep-th]].
- [29] B. Eden, P. Heslop, G. P. Korchemsky and E. Sokatchev, “The super-correlator/super-amplitude duality: Part I,” arXiv:1103.3714 [hep-th].
- [30] B. Eden, P. Heslop, G. P. Korchemsky and E. Sokatchev, “The super-correlator/super-amplitude duality: Part II,” arXiv:1103.4353 [hep-th].
- [31] E. I. Buchbinder and A. A. Tseytlin, “Semiclassical correlators of three states with large S^5 charges in string theory in $AdS_5 \times S^5$,” Phys. Rev. D **85**, 026001 (2012) [arXiv:1110.5621 [hep-th]].